JCI The Journal of Clinical Investigation

Targeting the XIAP/caspase-7 complex selectively kills caspase-3–deficient malignancies

Yuan-Feng Lin, … , Michael Hsiao, Po-Huang Liang

J Clin Invest. 2013;123(9):3861-3875. https://doi.org/10.1172/JCI67951.

Research Article

Caspase-3 downregulation (CASP3/DR) in tumors frequently confers resistance to cancer therapy and is significantly correlated with a poor prognosis in cancer patients. Because CASP3/DR cancer cells rely heavily on the activity of caspase-7 (CASP7) to initiate apoptosis, inhibition of activated CASP7 (p19/p12-CASP7) by X-linked inhibitor of apoptosis protein (XIAP) is a potential mechanism by which apoptosis is prevented in those cancer cells. Here, we identify the pocket surrounding the Cys^{246} residue of p19/p12-CASP7 as a target for the development of a protein-protein interaction (PPI) inhibitor of the XIAP:p19/p12-CASP7 complex. Interrupting this PPI directly triggered CASP7-dependent apoptotic signaling that bypassed the activation of the apical caspases and selectively killed CASP3/DR malignancies in vitro and in vivo without adverse side effects in nontumor cells. Importantly, CASP3/DR combined with p19/p12-CASP7 accumulation correlated with the aggressive evolution of clinical malignancies and a poor prognosis in cancer patients. Moreover, targeting of this PPI effectively killed cancer cells with multidrug resistance due to microRNA let-7a-1–mediated CASP3/DR and resensitized cancer cells to chemotherapy-induced apoptosis. These findings not only provide an opportunity to treat CASP3/DR malignancies by targeting the XIAP:p19/p12-CASP7 complex, but also elucidate the molecular mechanism underlying CASP3/DR in cancers.

Targeting the XIAP/caspase-7 complex selectively kills caspase-3–deficient malignancies

Yuan-Feng Lin,[1] Tsung-Ching Lai,[2] Chih-Kang Chang,[1] Chi-Long Chen,[3] Ming-Shyan Huang,[4] Chih-Jen Yang,[4] Hon-Ge Liu,[1] Jhih-Jhong Dong,[5] Yi-An Chou,[5] Kuo-Hsun Teng,[1] Shih-Hsun Chen,[6] Wei-Ting Tian,[5] Yi-Hua Jan,[2] Michael Hsiao,[2] and Po-Huang Liang[1,5]

[1]Institute of Biological Chemistry and [2]Genomics Research Center, Academia Sinica, Taipei, Taiwan. [3]Department of Pathology, Wan Fang Hospital, Taipei Medical University, Taipei, Taiwan. [4]Division of Pulmonary and Critical Care Medicine, Department of Internal Medicine, Kaohsiung Medical University Hospital, Kaohsiung Medical University, Kaohsiung, Taiwan. [5]Institute of Biochemical Sciences, National Taiwan University, Taipei, Taiwan. [6]Department of Biological Science and Technology, National Chiao Tung University, Hsin-Chu, Taiwan.

Caspase-3 downregulation (CASP3/DR) in tumors frequently confers resistance to cancer therapy and is significantly correlated with a poor prognosis in cancer patients. Because CASP3/DR cancer cells rely heavily on the activity of caspase-7 (CASP7) to initiate apoptosis, inhibition of activated CASP7 (p19/p12-CASP7) by X-linked inhibitor of apoptosis protein (XIAP) is a potential mechanism by which apoptosis is prevented in those cancer cells. Here, we identify the pocket surrounding the Cys^{246} residue of p19/p12-CASP7 as a target for the development of a protein-protein interaction (PPI) inhibitor of the XIAP:p19/p12-CASP7 complex. Interrupting this PPI directly triggered CASP7-dependent apoptotic signaling that bypassed the activation of the apical caspases and selectively killed CASP3/DR malignancies in vitro and in vivo without adverse side effects in nontumor cells. Importantly, CASP3/DR combined with p19/p12-CASP7 accumulation correlated with the aggressive evolution of clinical malignancies and a poor prognosis in cancer patients. Moreover, targeting of this PPI effectively killed cancer cells with multidrug resistance due to microRNA let-7a-1–mediated CASP3/DR and resensitized cancer cells to chemotherapy-induced apoptosis. These findings not only provide an opportunity to treat CASP3/DR malignancies by targeting the XIAP:p19/p12-CASP7 complex, but also elucidate the molecular mechanism underlying CASP3/DR in cancers.

Introduction

Caspase-3 (CASP3) is a major executioner protein of proteolytic degradation during apoptosis. Most cancer therapies, including radiotherapy, chemotherapy, and targeted therapy, induce extrinsic death receptor/CASP8/10–dependent and intrinsic mitochondria/CASP9–dependent apoptotic signals, which ultimately converge to activate CASP3 and promote cancer cell apoptosis. CASP3 downregulation (CASP3/DR), a progressive phenomenon that enables cancer cells to survive cancer therapy–induced apoptosis, has been observed in many malignancies and correlates significantly with poor survival in patients with solid tumors (1–11) and leukemia (12). In fact, insufficient induction of the apoptotic machinery is observed in CASP3/DR cancer cells treated with anticancer agents. Because these malignant cancer cells often develop drug resistance (9, 12, 13), an effective strategy to combat CASP3/DR in malignancies is urgently needed.

X-linked inhibitor of apoptosis protein (XIAP) belongs to the IAP family and tightly regulates the apoptotic and nonapoptotic caspase functions via interaction with the activated forms of the executioner caspases — namely, CASP3 and CASP7 — in mammalian cells (14). Under normal circumstances, IAPs ensure that low-level caspase activity does not erroneously initiate an apoptotic response either through incidental activation or as a consequence of nonapoptotic functions, such as proliferation (15), differentiation (16), and cytoskeletal remodeling (17). Once cells are committed to apoptosis, the mitochondria release the second mitochondria-derived activator of caspase/direct IAP-binding protein with low PI (SMAC/DIABLO) to relieve the XIAP-mediated inhibition of activated CASP3. Subsequently, this reaction triggers activation of CASP7 to promote apoptotic proteolysis (18). In normal cells, XIAP predominantly inhibits CASP3 activation because it both mediates caspase-associated cellular functions (19) and regulates CASP7 activation (20). However, cancer cells that downregulate CASP3 expression to escape from apoptosis may upregulate the structurally and functionally similar CASP7 (18, 21, 22) to achieve cellular homeostasis (23, 24), although the mechanism remains unclear. Staurosporine (STS), an inducer of the intrinsic mitochondrial apoptotic pathway, appears to inefficiently elevate intracellular CASP7 activity and induce apoptosis in embryonic fibroblasts derived from *Casp3*-knockout mice (14) and *CASP3*-null MCF-7 breast cancer cells (25), even in the presence of SMAC/DIABLO. These results are consistent with those from in vitro binding assays demonstrating that SMAC/DIABLO is unable to block the protein-protein interaction (PPI) between XIAP and the Ala-Lys-Pro (AKP) motif of activated CASP7 (composed of the p19 and p12 subunits; referred to herein as p19/p12-CASP7) (26). Because the XIAP:p19/p12-CASP7 complex accumulates in STS-treated MCF-7 cells, the PPI between XIAP and p19/p12-CASP7 is thought to be the mechanism of chemoresistance in CASP3/DR cancer cells (25). Although recent studies have used MCF-7 cells as a model to assess new therapeutic strategies for overcoming CASP3/DR-associated chemoresistance (27–29), our present study is the first to propose a strategy to specifically inhibit the PPI between XIAP and p19/p12-CASP7 to achieve anticancer activity against CASP3/DR malignancies.

Conflict of interest: The authors have declared that no conflict of interest exists.
Citation for this article: *J Clin Invest.* 2013;123(9):3861–3875. doi:10.1172/JCI67951.

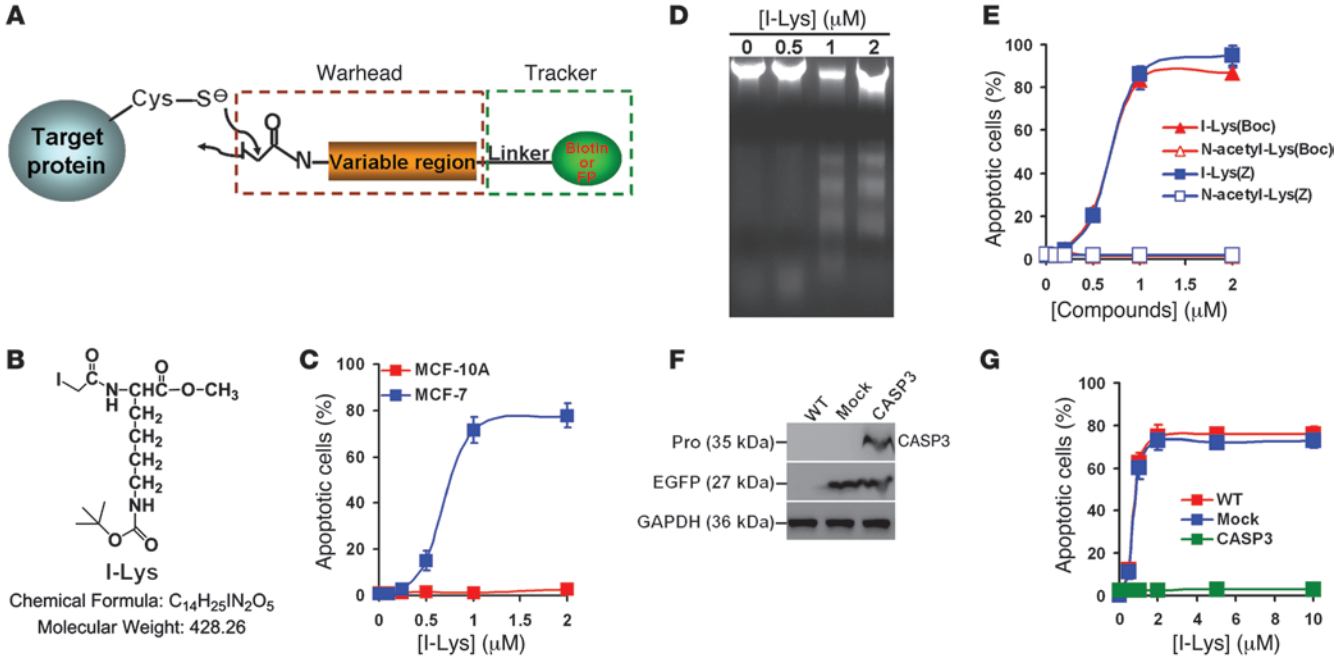

Figure 1

Cytotoxicity-based screening of synthetic I-AAs against *CASP3*-null MCF-7 breast cancer cells. (**A**) Experimental strategy for identifying new drug targets using I-AAs. (**B**) Structure of I-Lys. (**C**) Cytocidal effects of I-Lys on MCF-7 cells and normal MCF-10A mammary epithelium cells. Cells were treated with I-Lys at the indicated concentrations for 24 hours. Accumulation of cells in the sub-G_0 fraction was determined by PI-based flow cytometric analysis. (**D**) Fragmentation of chromosomal DNA in response to the indicated I-Lys concentrations 24 hours after treatment. (**E**) Apoptosis in MCF-7 cells treated with I-Lys analogs with diverse protection groups or without the iodo-group (BOC, butyloxycarbonyl; Z, benzyloxycarbonyl) at the indicated doses for 24 hours. (**F**) Immunoblotting of pro-CASP3 in WT, mock-transfected (pIRES-EGFP vector only), or CASP3-transfected (containing pIRES-EGFP vector) MCF-7 cells. GAPDH was used as an internal control for protein loading. EGFP was used as a control for the transfection procedure. (**G**) Apoptosis in cells as in **F** after exposure to I-Lys at the indicated doses for 24 hours. (**C**, **E**, and **G**) Data (mean ± SD) are from 3 independent experiments.

By performing MCF-7 cell–based cytotoxicity assays, we found that N-iodoacetyl-Lys-tert-butyloxycarbonyl (N-iodoacetyl-Lys[BOC]; referred to herein as I-Lys), in a synthetic compound library designed for targeting PPIs, was capable of directly disrupting the intracellular XIAP:p19/p12-CASP7 complexes by alkylating the Cys^{246} residue of CASP7, which promptly released p19/p12-CASP7 from the complex, subsequently promoted poly (ADP-ribose) polymerase (PARP) processing, and ultimately caused DNA fragmentation and apoptosis in CASP3/DR breast cancer cells. We also found that the XIAP:p19/p12-CASP7 complex was constitutively present in nonapoptotic CASP3/DR cancer cells and inversely correlated with CASP3 expression, thereby providing a basis for the cytotoxic specificity of I-Lys against CASP3/DR cancer cells in vitro and in vivo. Moreover, our results demonstrated that CASP3/DR and p19/p12-CASP7 accumulation correlated with poor prognosis in clinical cohorts with breast, lung, and colon cancers. This correlation is likely due to the development of drug resistance, as I-Lys effectively killed multidrug-resistant breast cancer cells by disrupting the XIAP:p19/p12-CASP7 complex. Additionally, low doses of I-Lys synergistically enhanced the tumoricidal efficacy of anticancer agents on CASP3/DR malignancies. Therefore, targeting the XIAP:p19/p12-CASP7 complex could be an effective, specific, and safe strategy to treat CASP3/DR malignancies.

Results

Cytotoxic screening of synthetic iodoacetyl amino acids against CASP3-null MCF-7 cells. PrognoScan analysis of *CASP3* gene expression in publicly available microarray databases revealed that CASP3/DR correlated with cancer metastasis and recurrence and predicted poor overall and disease-free survival rates in clinical cohorts with diverse cancers (Supplemental Table 1; supplemental material available online with this article; doi:10.1172/JCI67951DS1). Immunohistochemical (IHC) staining of CASP3 in clinical breast, lung, and colon cancer specimens supported the hypothesis that CASP3/DR contributes to the reduced incidence of disease-free survival (Supplemental Figure 1, A–C). These findings prompted us to identify PPIs as a target for the treatment of CASP3/DR malignancies using the *CASP3*-null MCF-7 breast cancer cell line as a cell-based model. Because PPIs are mediated by amino acids, we previously generated a series of iodoacetyl amino acids (I-AAs), which form covalent bonds with Cys residues in their target proteins, with the aim of discovering a new anticancer drug target (30, 31). In this strategy, a fluorescent probe and biotin are used to visualize and recover the target protein by avidin-based affinity chromatography, respectively (Figure 1A). Here, we performed MCF-7 cell–based cytotoxicity assays to screen synthetic I-AAs and found that I-Lys (Figure 1B) exhibited the greatest cytotoxic effect in MCF-7 cells at a concentration of 1 μM (Supplemental Figure 2). Furthermore, we found that I-Lys efficiently killed

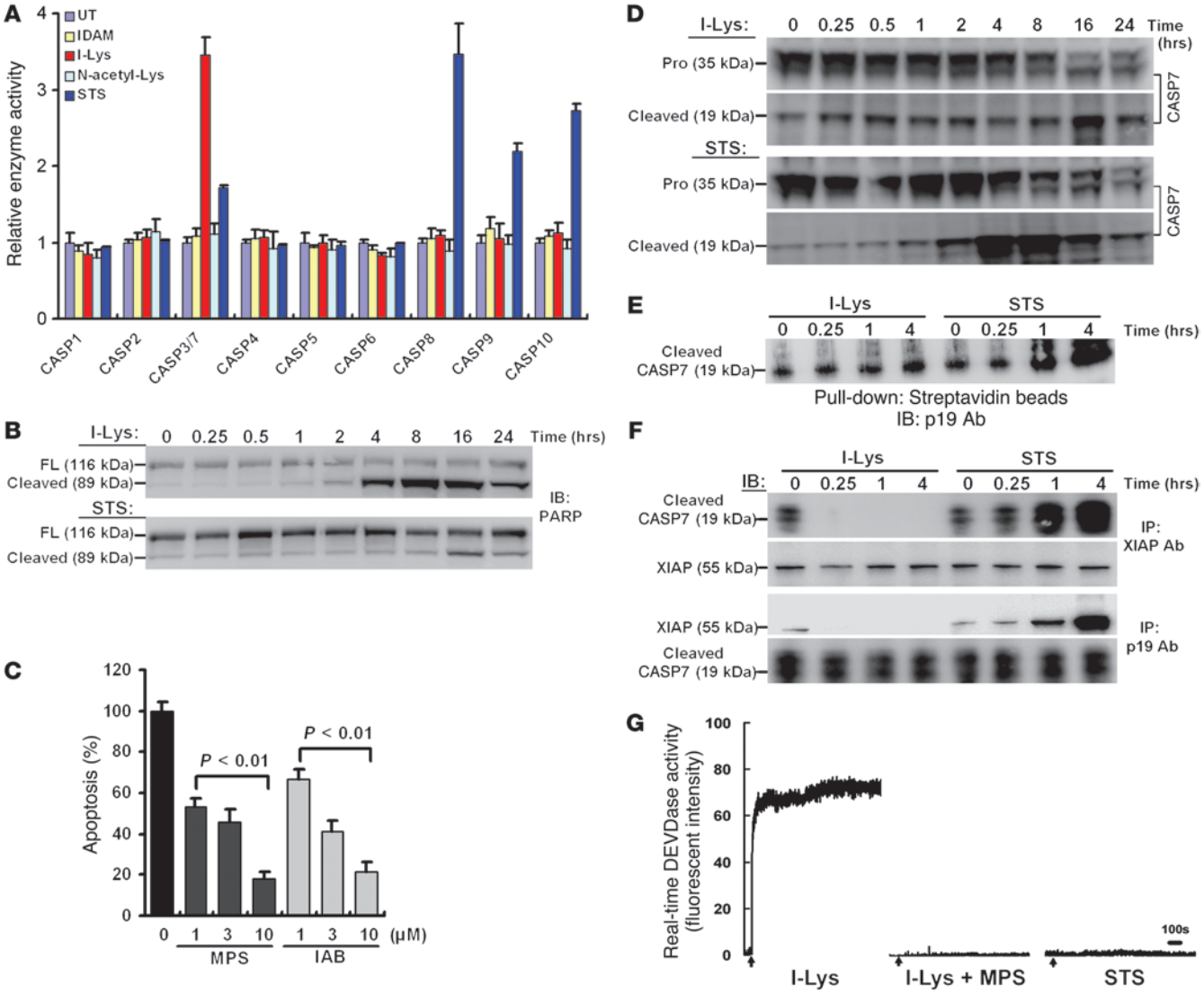

Figure 2

I-Lys directly triggers CASP7-mediated apoptotic signaling by disrupting the XIAP:p19/p12-CASP7 complex in MCF-7 cells. (**A**) Determination of intracellular caspase activity in untreated (UT) MCF-7 cells or in MCF-7 cells treated with IDAM, N-acetyl-Lys, I-Lys, or STS (1 μM each) for 24 hours. (**B**) Immunoblotting for the full-length (FL) and cleaved forms of PARP in MCF-7 cells treated with 1 μM I-Lys for the indicated times. (**C**) Apoptosis in MCF-7 cells treated with 1 μM I-Lys for 24 hours in the presence or absence of the CASP7 inhibitor MPS or the PARP inhibitor IAB at the indicated doses. (**D**–**F**) Immunoblotting for pro-CASP7 and p19/p12-CASP7 (**D**), tracing p19/p12-CASP7 by biotin-VAD (**E**), and immunoprecipitation/Western blot analysis of XIAP:p19/p12-CASP7 complexes (**F**) in MCF-7 cells treated with I-Lys or STS (1 μM each) for the indicated times. (**G**) Real-time DEVDase activity in MCF-7 cells treated with I-Lys (1 μM), in the absence or presence of MPS (10 μM), or with STS (1 μM). I-Lys or STS were added to the medium 50 seconds after the onset of the experiment. Scale bar: 100 seconds. (**A** and **C**) Data are mean ± SEM.

MCF-7 cells (EC_{50} 0.64 μM), but not normal MCF-10A breast epithelium cells, in both short- and long-term cytotoxicity assays (Figure 1C and Supplemental Figure 3), which suggests that this compound has selective anticancer activity. The observed chromosomal DNA fragmentation (Figure 1D) indicated that I-Lys caused cell death in MCF-7 cells through the intracellular apoptotic machinery. The removal of an iodo-group completely abolished the cytocidal effect of I-Lys, but changing the protective group from butyloxycarbonyl to benzyloxycarbonyl on the Lys side chain did not significantly alter the cytocidal effect (Figure 1E and Supplemental Figure 4), which indicates that the formation of an adduct between I-Lys and Cys on the target protein is required for I-Lys–elicited apoptotic signaling. Interestingly, reconstitution of CASP3 expression in MCF-7 cells abolished the cytocidal effect of I-Lys (Figure 1, F and G), which suggests that I-Lys selectively kills CASP3/DR cancer cells.

I-Lys directly disrupts the XIAP:p19/p12-CASP7 complex, leading to CASP7-mediated apoptotic signaling that bypasses the activation of its upstream effector caspases. Because I-Lys caused cell death through apoptotic signaling, we determined the activation state of the cas-

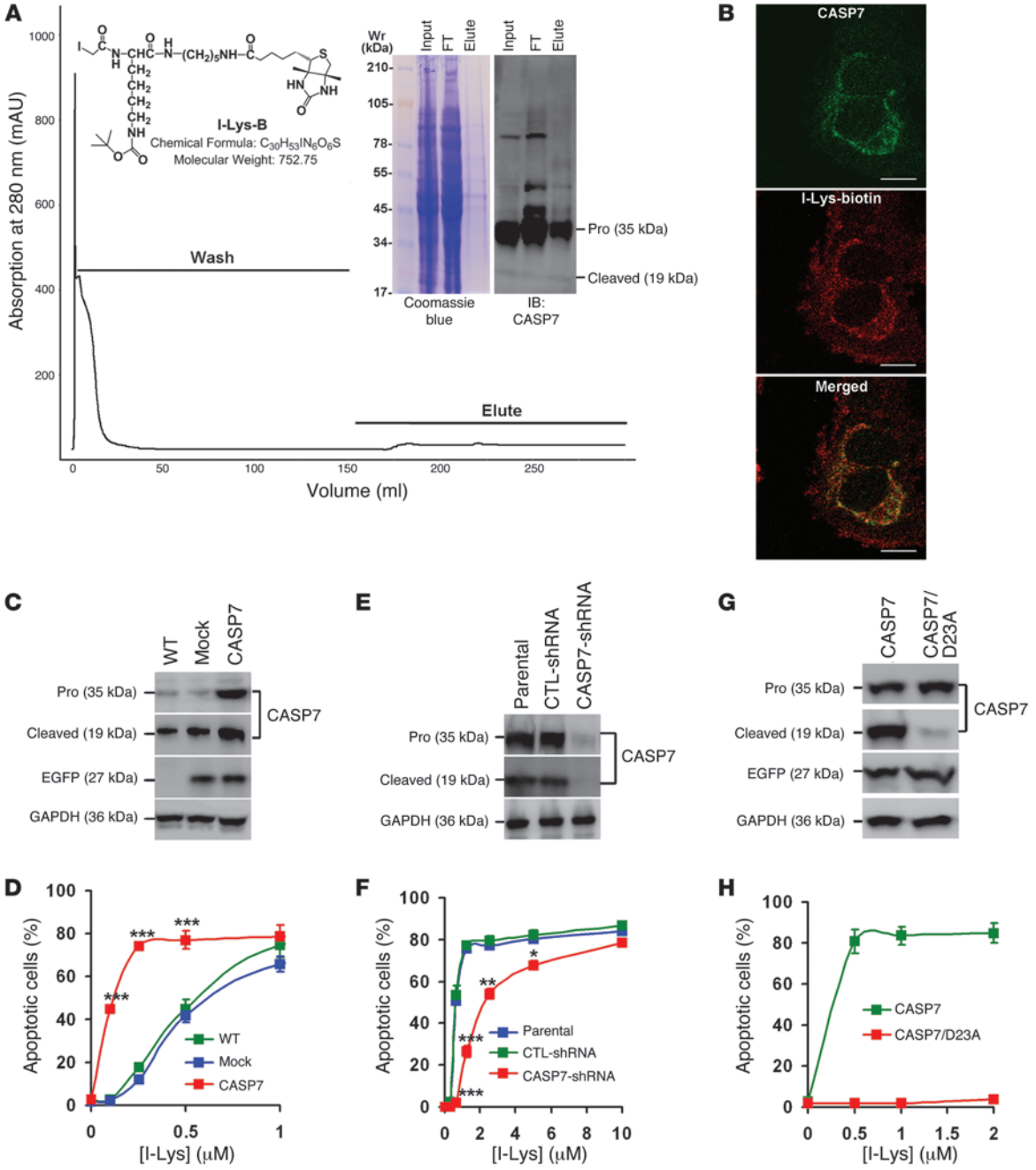

Figure 3

Identification of CASP7 as a target for I-Lys. (**A**) Isolation of I-Lys-B–labeled proteins from MCF-7 cell lysates. Top left: Structure of I-Lys-B. Top right: streptavidin-affinity chromatography of I-Lys-B–interacting protein in MCF-7 cell lysates and immunoblotting for pro-CASP7 and p19/p12-CASP7 in the MCF-7 cell lysates (input), flow-through (FT), and eluted fractions. (**B**) Confocal microscopy of I-Lys-B–labeled MCF-7 cells. A rhodamine-conjugated streptavidin agent was used to trace intracellular I-Lys-B. Intracellular CASP7 was immunostained with a CASP7-specific antibody in conjunction with a FITC-conjugated secondary antibody. Scale bars: 20 μm. Original magnification, ×400. (**C**–**H**) Immunoblotting for pro-CASP7, p19/p12-CASP7, EGFP (control for cell transfection), and GAPDH (control for protein loading) (**C**, **E**, and **G**) and I-Lys–induced apoptosis (**D**, **F**, and **H**) in MCF-7 cells transfected with WT, mock, or CASP7 (**C** and **D**); WT, control shRNA, or CASP7 shRNA (**E** and **F**); or CASP7 or CASP7/D23A (**G** and **H**). (**D**, **F**, and **H**) Data (mean ± SEM) are from 3 independent experiments. $^{*}P < 0.05$, $^{**}P < 0.01$, $^{***}P < 0.001$.

pases involved in the extrinsic and intrinsic apoptotic pathways in MCF-7 cells. Our data showed that only CASP7 activity was detected in MCF-7 cells after treatment with I-Lys for 24 hours (Figure 2A). The insensitivity of other caspases to I-Lys treatment was not due to loss of their expression in MCF-7 cells, as shown by Western blot (Supplemental Figure 5). Iodoacetamide (IDAM) and N-acetyl-Lys treatment in MCF-7 cells did not promote caspase activation, which demonstrated the requirement of I-Lys binding

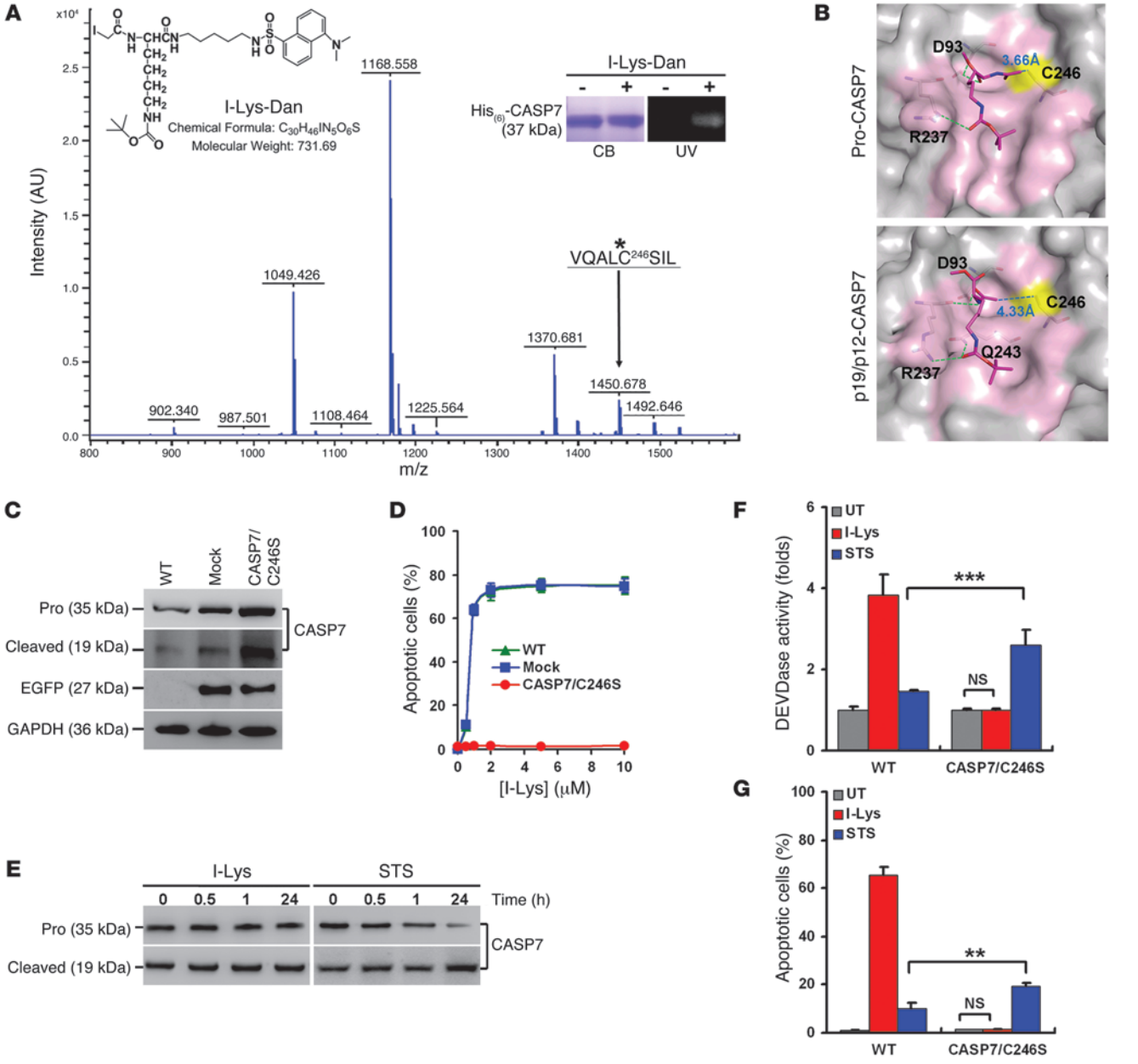

Figure 4

Alkylation of the Cys[246] residue of CASP7 by I-Lys. (**A**) Mass spectrometric analysis of I-Lys-Dan–labeled CASP7. The arrow denotes a peak with a molecular weight corresponding to the VQALCSIL peptide fragment bound to Lys-Dan at the Cys[246] residue. Top left: Structure of I-Lys-Dan. Top right: SDS-PAGE analysis of recombinant His-tagged CASP7, labeled with or without I-Lys-Dan, by Coomassie blue (CB) staining or under UV light. (**B**) Molecular docking of I-Lys (stick) into a region (pink surface) near the Cys[246] residue (yellow surface) of pro-CASP7 (PDB 1K86) or p19/p12-CASP7 (PDB 1I51). Green dashed lines indicate the formation of intermolecular H-bonds. (**C**) Western blot analysis of CASP7, EGFP, and GAPDH using their specific antibodies in WT, mock-transfected, and CASP7/C246S-transfected MCF-7 cells. (**D**) Apoptosis in 1 μM I-Lys–treated WT, mock, and CASP7/C246S MCF-7 cells. (**E**) Immunoblotting for pro-CASP7 processing in CASP7/C246S MCF-7 cells treated with I-Lys or STS (1 μM each) for 24 hours. (**F** and **G**) Intracellular DEVDase activity (**F**) and apoptosis (**G**) in WT or CASP7/C246S MCF-7 cells that were untreated or treated with 1 μM I-Lys or STS for 24 hours. Data (mean ± SEM) are from 3 independent experiments. $^{**}P < 0.01$, $^{***}P < 0.001$.

specificity and alkylating reactivity in this event. STS treatment increased the activity of CASP7, CASP8, CASP9, and CASP10 (Figure 2A), which suggests that I-Lys treatment may not induce the activation of extrinsic and intrinsic caspase-dependent apoptotic pathways. Proteolysis of poly (ADP-ribose) polymerase (PARP) — a downstream effector of CASP7 in the demolition phase of apoptosis (32), chromosomal DNA fragmentation, and apoptosis — was also detected in I-Lys–treated MCF-7 cells in a time-dependent manner (Figure 2B and Supplemental Figure 6, A and B). Compared with I-Lys, STS treatment promoted weak induction of

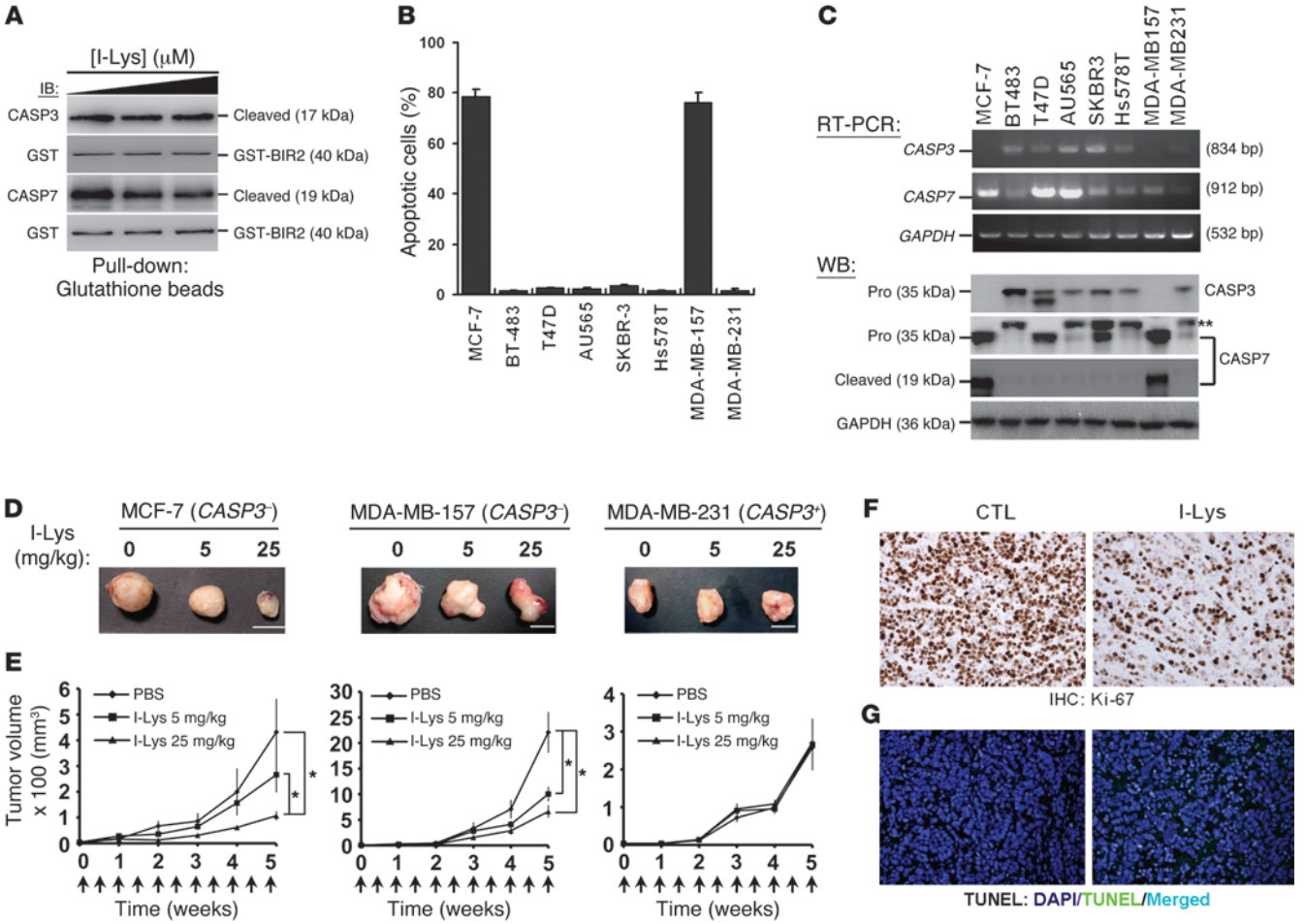

Figure 5

Anticancer effectiveness of targeting the XIAP:p19/p12-CASP7 complex in vitro and in vivo. (**A**) In vitro binding assay for XIAP (GST-tagged linker-BIR2 domain) interaction with the cleaved form of CASP3 or p19/p12-CASP7, in the presence of increasing I-Lys concentrations (0, 0.1, and 0.5 mM). (**B**) Cell apoptosis in a panel of breast cancer cell lines treated with 1 μM I-Lys at for 24 hours. Data (mean ± SEM) are from 3 independent experiments. (**C**) RT-PCR analysis for *CASP3*, *CASP7*, and *GAPDH* expression and Western blot (WB) analysis for pro-CASP3, pro-CASP7, p19/p12-CASP7, and GAPDH in various breast cancer cells. The symbol ** represents a nonspecific reaction of CASP7 antibody. (**D** and **E**) Tumor mass (**D**) and volume (**E**) from MCF-7, MDA-MB-157, and MDA-MB-231–xenografted mice treated with PBS control (n = 8) or with I-Lys at 5 (n = 6) and 25 (n = 8) mg/kg for 5 weeks. Arrows indicate the time points of I-Lys administration. *P < 0.05 versus PBS, 1-way ANOVA and Duncan's multiple range test. (**F** and **G**) Ki-67 immunostaining (**F**; brown) and TUNEL assay (**G**; green) of MCF-7 tumor tissues derived from mice treated without or with 25 mg/kg I-Lys. Nuclei in **G** were stained with DAPI (blue). Original magnification, ×200.

CASP7-mediated PARP cleavage (Figure 2B) and apoptosis (33) in MCF-7 cells during the time course, presumably due to sequestration of p19/p12-CASP7 by XIAP (25). Pharmaceutical inhibition of the CASP7/PARP signaling axis by their respective inhibitors, 5-[(S)-(+)-2-(methoxymethyl)pyrrolidino]sulfonylisatin (MPS) (34) and 5-iodo-6-amino-1,2-benzopyrone (IAB), suppressed I-Lys–induced apoptosis in MCF-7 cells in a dose-dependent manner (Figure 2C). These results demonstrated a requirement for CASP7 activity in I-Lys–dependent apoptosis in MCF-7 cells. Furthermore, we detected proteolytic processing of CASP7 in response to I-Lys treatment in MCF-7 cells. Although STS, which is known to elicit caspase-dependent apoptosis in MCF-7 cells (33), effectively promoted the processing of pro-CASP7 into p19/p12-CASP7, reaching a maximal level at 8 hours after treatment, I-Lys did not affect the proteolytic cleavage of pro-CASP7 within 8 hours of treatment (Figure 2D). However, pro-CASP7 was processed into p19/p12-CASP7 after 16 hours of treatment with I-Lys in MCF-7 cells (Figure 2D). Labeling of active p19/p12-CASP7 by biotinylated VAD clearly showed that treatment with STS, but not I-Lys, dramatically increased the intracellular levels of p19/p12-CASP7 at the onset of treatment (≤4 hours) in MCF-7 cells (Figure 2E). In contrast to STS, I-Lys did not induce CASP9 processing in MCF-7 cells (Supplemental Figure 7). These findings suggest that I-Lys–induced CASP7 activation may be uncoupled from pro-CASP7 activation. Therefore, we determined whether I-Lys directly disrupts the intracellular XIAP:p19/p12-CASP7 complex to induce apoptosis in MCF-7 cells. Immunoprecipitation analysis revealed that I-Lys reduced the level of the intracellular XIAP:p19/p12-CASP7 complex within 15 minutes of treatment, whereas STS treatment promoted XIAP:p19/p12-CASP7 complex

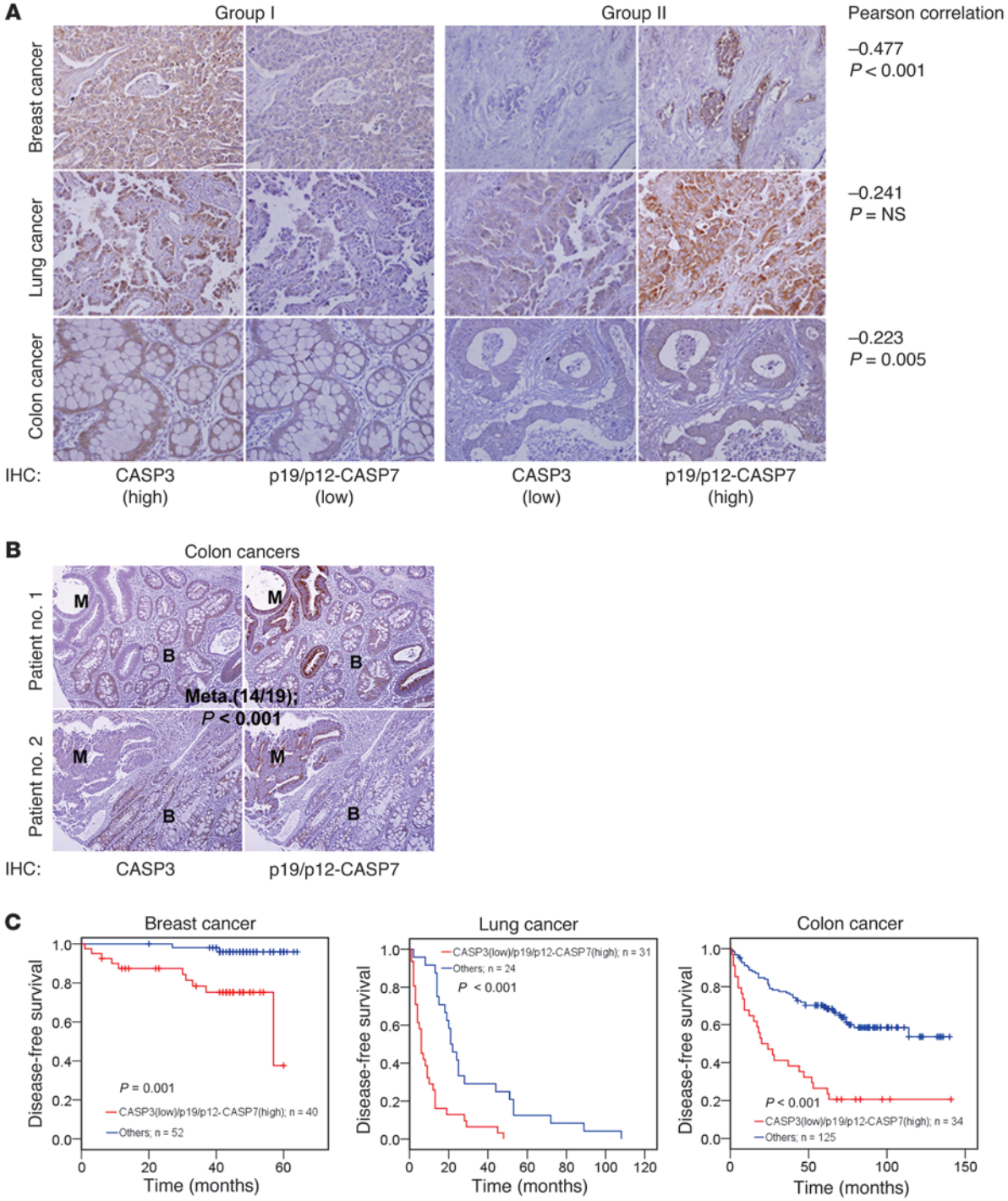

Figure 6

p19/p12-CASP7 accumulates in CASP3/DR malignancies and is closely associated with disease progression. (**A**) IHC analysis of CASP3 and p19/p12-CASP7 expression in 2 representative groups of clinical breast, lung, and colon cancer specimens. Original magnification, ×400. *R* values and statistical significance, calculated using Pearson correlation analysis, are shown at right. Negative *R* values indicate that CASP3 and p19/p12-CASP7 expression levels are inversely correlated in clinical cancer samples. (**B**) IHC analysis of CASP3 and p19/p12-CASP7 expression in 2 serial sections of representative colon cancer tissue. Morphologically benign (B) and malignant (M) regions are indicated. Original magnification, ×200. (**C**) Kaplan-Meier analyses of survival probabilities in cohorts of patients with breast, lung, and colon cancer expressing combined low-level CASP3 and high-level p19/p12-CASP7 compared with other signatures. Log-rank tests were used to determine statistical significance.

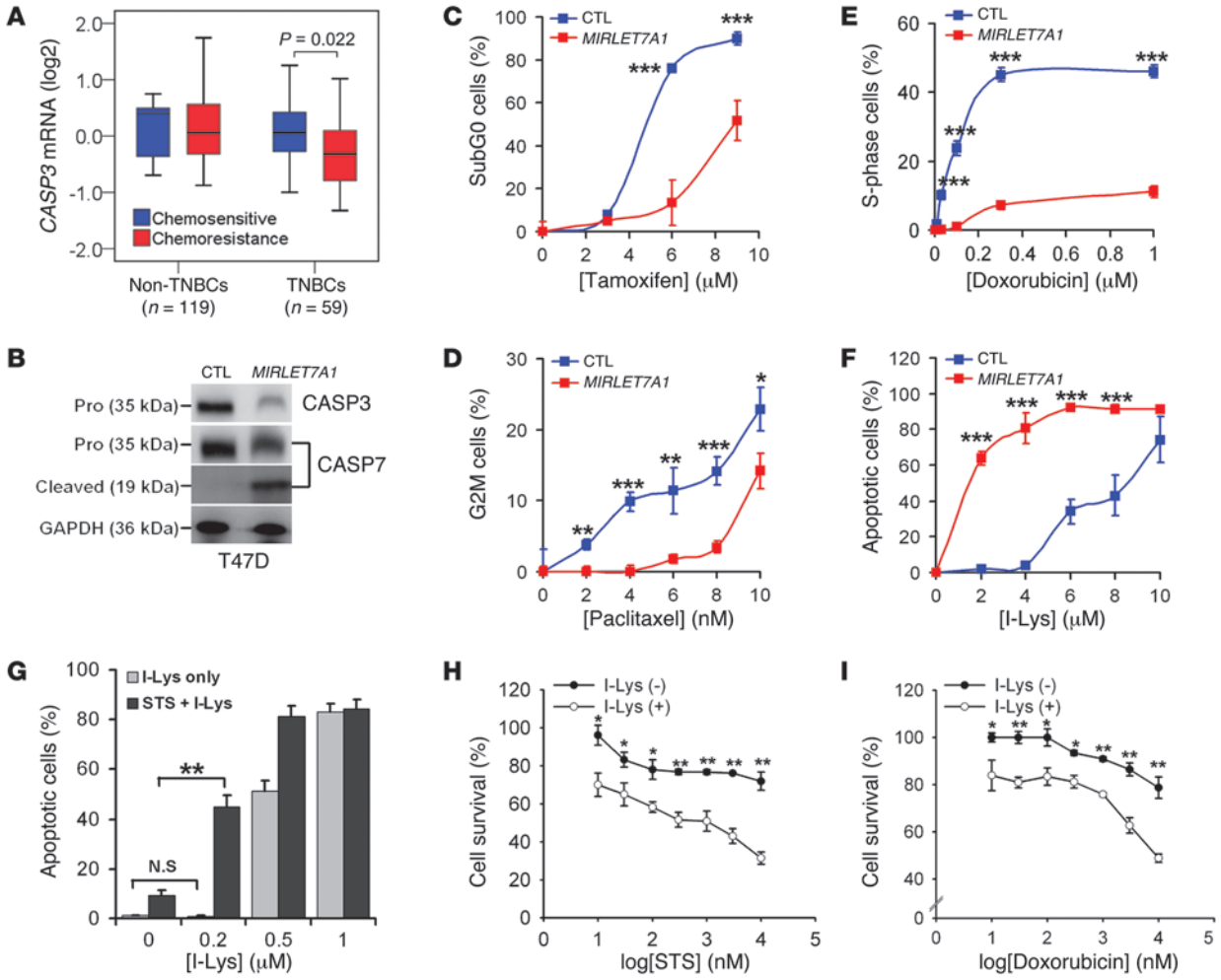

Figure 7

I-Lys selectively kills cancer cells with multidrug resistance and effectively sensitizes chemoresistant cancer cells to chemotherapy. (**A**) *CASP3* mRNA levels in non-TNBC and TNBC clinical specimens with or without chemoresistance. (**B**) Immunoblotting of pro-CASP3, pro-CASP7, and p19/p12-CASP7 in T47D breast cancer cells stably overexpressing a nontargeted control or *MIRLET7A1*. GAPDH was used as an internal control for protein loading. (**C**–**F**) Chemosensitivity of control and *MIRLET7A1*-expressing T47D cells to tamoxifen (**C**), paclitaxel (**D**), doxorubicin (**E**), and I-Lys (**F**). After 24 hours of incubation, the fraction of cells in the sub-G_0, G2/M, or S phases in each treatment was determined using PI-based flow cytometric analysis. (**G**–**I**) Effect of I-Lys on enhancing STS- or doxorubicin-induced apoptosis in MCF-7 cells. Cells were (**G**) pretreated with I-Lys at the indicated concentrations for 1 hour prior to treatment with STS at 1 μM for 24 hours or were (**H** and **I**) preincubated with I-Lys 0.2 μM for 1 h prior to treatment with STS (**H**) or doxorubicin (**I**) at the indicated concentrations for 24 hours. The extent of cell viability was determined by MTT assay. (**C**–**I**) Data (mean ± SEM) are from 3 independent experiments. **P* < 0.05, ***P* < 0.01, ****P* < 0.001.

formation through pro-CASP7 activation (Figure 2F). Real-time determination of CASP7 DEVDase activity revealed that I-Lys induced a rapid increase in intracellular CASP7 activity within a few seconds of administration; this effect was abolished by preincubating MCF-7 cells with MPS (Figure 2G). In contrast, STS treatment induced only a minor increase in intracellular CASP7 activity several minutes after treatment (Figure 2G). The D148A, E219R, and H223V mutations in XIAP together have been shown to be important for intermolecular interaction between XIAP and p19/p12-CASP7 and between XIAP and active CASP3 (35); however, the D148A mutation alone robustly alters the inhibitory effects of XIAP on the activity of CASP3, but not p19/p12-CASP7 (35). An XIAP mutant containing all 3 mutations, but not an XIAP containing D148A mutation alone, enhanced STS-induced apoptosis in MCF-7 cells (Supplemental Figure 8). These results clearly demonstrated that removal of XIAP inhibition on active p19/p12-CASP7 by I-Lys is a key process for eliciting CASP7-mediated apoptotic signaling cascades in *CASP3*-null MCF-7 cells.

I-Lys binds to pro-CASP7 and p19/p12-CASP7, but not XIAP. To verify that I-Lys is capable of interacting with CASP7 in MCF-7 cells, we synthesized biotinylated I-Lys (I-Lys-B) and used it to identify I-Lys–interacting proteins via streptavidin-affinity chromatography (Figure 3A). Although mass spectroscopic analysis revealed the presence of several proteins, in addition to CASP7, that were likely bound to I-Lys (Supplemental Table 2), none of these interactions led to CASP7 activation. Our data showed that pro-CASP7 and p19/p12-CASP7, but not XIAP, were detected in the chromatography eluates by immunoblotting with their respective antibodies

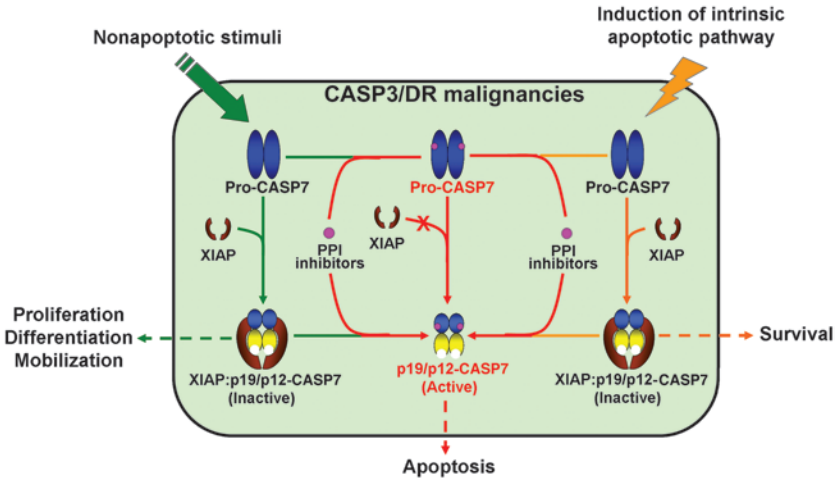

Figure 8
Proposed pathway for disrupting the XIAP:p19/p12-CASP7 complex in CASP3/DR malignancies, and a chemotherapeutic strategy for targeting the XIAP:p19/p12-CASP7 complex and pro-CASP7 with I-Lys to directly kill tumor cells or sensitize CASP3/DR malignancies to chemotherapy.

(Figure 3A and Supplemental Figure 9). Confocal microscopy also revealed that I-Lys-B colocalized with CASP7 in the cytoplasm of MCF-7 cells (Figure 3B). These results demonstrated that I-Lys can bind directly to p19/p12-CASP7, thereby inhibiting PPI with XIAP.

Forced expression of CASP7 in MCF-7 cells enhanced p19/p12-CASP7 production and potentiated the cytocidal effect of I-Lys (Figure 3, C and D). In contrast, restoring CASP3 expression in MCF-7 cells diminished p19/p12-CASP7 accumulation (Supplemental Figure 10), thereby desensitizing the cells to I-Lys–mediated apoptosis (Figure 1G). Furthermore, shRNA knockdown of CASP7 reduced p19/p12-CASP7 production and consequently decreased I-Lys–induced apoptosis in MCF-7 cells (Figure 3, E and F). Accordingly, ectopic expression of mutant CASP7 bearing a D23A mutation (referred to herein as CASP7/D23A), which enhanced pro-CASP7 expression but obstructed the production of p19/p12-CASP7, abrogated the cytotoxic effect of I-Lys in MCF-7 cells (Figure 3, G and H). These findings indicate that p19/p12-CASP7 is a key target for inducing apoptosis by I-Lys and is constitutively produced by *CASP3*-null MCF-7 cells to compensate for the lack of CASP3-mediated nonapoptotic responses (24).

I-Lys alkylates the Cys^{246} residue of CASP7. To ascertain which key Cys residue is alkylated by I-Lys, thereby preventing XIAP-mediated inhibition of activated p19/p12-CASP7, we synthesized a dansylated I-Lys (I-Lys-Dan) compound to visualize its adduct with a recombinant CASP7 protein under UV light (Figure 4A). Both I-Lys and I-Lys-B inhibited the incorporation of I-Lys-Dan into CASP7 (Supplemental Figure 11), which indicates that neither the dansyl nor biotin groups, which are separated by a linker, interfered with the binding of I-Lys toward the Cys^{246} residue of CASP7. Mass spectroscopic analysis revealed that the Cys^{246} residue within the CASP7 peptide fragment VQALCSIL was modified by I-Lys-Dan, as demonstrated by the peak at *m/z* 1,450.678 (Figure 4A), equal to the predicted mass value of the VQALCSIL peptide fragment (*m/z* 846.4753) with a Lys-Dan group (*m/z* 604.7955). Molecular docking analysis revealed that I-Lys was positioned such that the iodo-bearing carbon was 3.66 and 4.33 Å away from the Cys^{246} thiol atom of pro-CASP7 and p19/p12-CASP7, respectively (Figure 4B). This distance is suitable for covalent bond formation with Cys^{246}, but would preclude interaction with the catalytic Cys^{186} residue. Furthermore, circular dichroism spectroscopic analysis revealed that I-Lys incorporation did not cause dramatic changes in the secondary structure of the p19/p12-CASP7 protein (Supplemental Figure 12), which supports the hypothesis that I-Lys specifically interrupts the PPI within the XIAP:p19/p12-CASP7 complex without affecting CASP7 activity.

To determine whether alkylation of Cys^{246} in CASP7 by I-Lys is solely responsible for inducing the apoptosis in MCF-7 cells, we generated an MCF-7 cell line stably expressing a mutant CASP7 bearing a C246S mutation (CASP7/C246S; Figure 4C). As expected, I-Lys failed to cause apoptosis in CASP7/C246S-expressing MCF-7 cells (Figure 4D), although STS could still induce CASP7-dependent apoptosis. Remarkably, STS, but not I-Lys, induced the processing of the C246S mutant pro-CASP7 into p19/p12-CASP7 (Figure 4E), which enhanced CASP7 activity and promoted an enhanced apoptotic response in CASP7/C246S-expressing versus WT MCF-7 cells (Figure 4, F and G). These data demonstrated that alkylation of the Cys^{246} residue by I-Lys is the key step for disrupting the XIAP:p19/p12-CASP7 complex and eliciting CASP7-dependent apoptotic signaling in *CASP3*-null MCF-7 cells.

I-Lys inhibits the PPI between XIAP and p19/p12-CASP7 but not active CASP3. Because CASP3 and CASP7 are functionally and structurally similar, and both are able to interact with the BIR2 domain of XIAP when activated (35), we performed an in vitro protein binding assay to verify the specificity of I-Lys for the PPI between XIAP and p19/p12-CASP7. We found that I-Lys disrupted XIAP BIR2 domain–mediated inhibition of p19/p12-CASP7, even in preformed complexes, but not of active CASP3 (Figure 5A). This selectivity may be attributed to the presence of an embedded thiol group in the corresponding Cys^{220} residue in CASP3, which does not react with I-Lys (Supplemental Figure 13). I-Lys was also capable of disrupting the binding of full-length XIAP with p19/p12-CASP7, but not with the C246S mutant p19/p12-CASP7 (Supplemental Figure 14, A and B), which supports the hypothesis that the alkylation of Cys^{246} in p19/p12-CASP7 and subsequent disruption of the PPI is responsible for MCF-7 cell apoptosis after I-Lys treatment.

I-Lys selectively kills CASP3/DR cancer cells in vitro and in vivo. We examined the selectivity of I-Lys in a panel of breast cancer cell lines, including estrogen receptor–positive (ER$^+$) cells (MCF-7, BT483, and T47D), HER2$^+$ cells (AU565 and SKBR3), and triple-negative breast cancer (TNBC) cells (Hs578T, MDA-MB-157, and MDA-MB-231). Our data showed that I-Lys selectively killed the ER$^+$ MCF-7 cells

and the TNBC MDA-MB-157 cells (Figure 5B). Similar to MCF-7 cells, MDA-MB-157 cells lacked *CASP3* expression and constitutively produced p19/p12-CASP7 (Figure 5C), which potentially explains the cytotoxic specificity of I-Lys toward these cells.

To test the in vivo tumoricidal effectiveness of targeting the XIAP:p19/p12-CASP7 complex with I-Lys in CASP3/DR malignancies, we transplanted *CASP3*-null (MCF-7 or MDA-MB-157) or *CASP3*-expressing (MDA-MB-231) breast cancer cells into immunodeficient mice. Intraperitoneal injection of I-Lys (5 or 25 mg/kg) into tumor-bearing mice dramatically inhibited the tumor growth and significantly reduced the tumor volume of CASP3/DR breast cancer cells (Figure 5, D and E). In contrast, I-Lys treatment failed to suppress the growth of MDA-MB-231 tumors (Figure 5, D and E). Histology revealed that I-Lys downregulated Ki-67 expression in tumor tissue (Figure 5F), demonstrating the inhibition of tumor cell proliferation. TUNEL assays showed that I-Lys–induced tumor cell death was mediated by the apoptotic machinery rather than necrosis (Figure 5G). Furthermore, serological examination revealed that I-Lys administration did not affect the liver (GOT/GTP) or renal (BUN/creatinine) function of tumor-bearing mice (Supplemental Figure 15A). Accordingly, no obvious changes in body weight or disorders of the heart, lung, liver, kidney, or spleen tissues from the experimental mice were detected during the course of I-Lys administration (Supplemental Figure 15, B and C). Administration of I-Lys at a 10-fold higher dose (250 mg/kg) to evaluate the maximum tolerated dose (MTD) (36) did not result in liver or kidney injuries or affect hepatic or renal function or body weight of the mice (Supplemental Figure 16, A–C). These findings demonstrated that I-Lys selectively inhibits the growth of CASP3/DR tumors without causing harmful side effects in tumor-bearing mice.

CASP3/DR is accompanied by accumulation of p19/p12-CASP7, which significantly correlates with cancer progression and poor prognosis in cancer patients. To determine whether CASP3/DR-mediated p19/p12-CASP7 accumulation occurs in clinical samples, and to validate our therapeutic strategy, we analyzed protein levels of CASP3 and p19/p12-CASP7 using IHC staining in serial sections of cancer tissue from breast, lung, and colon cancer patients (Figure 6A). Our results showed that CASP3 expression was inversely correlated with p19/p12-CASP7 accumulation in breast and colon cancers ($P < 0.01$; Figure 6A). In colon cancer tissue, CASP3/DR was accompanied by p19/p12-CASP7 accumulation in morphologically malignant tissue; this result was supported by statistical evidence that metastatic CASP3/DR colon cancers frequently expressed high levels of p19/p12-CASP7 (Figure 6B and Supplemental Figure 17A). Similar results were observed in the clinical specimens from patients with lung cancer (Supplemental Figure 17B). The frequency of CASP3/DR in the clinical specimens (59 of 92; 64.1%) was greater than what we observed in the cell lines (Figure 5B). Thus, we analyzed *CASP3* mRNA expression in normal MCF-10A cells and 45 additional breast cancer cell lines. Although MCF-10A cells expressed a normal level of *CASP3*, 35 of 45 (77.8%) breast cancer cell lines exhibited a downregulation in the level of *CASP3* mRNA (Supplemental Figure 18). This finding was consistent with our IHC data using clinical breast cancer samples obtained from the hospital in Taiwan. In contrast, CASP3/DR and p19/p12-CASP7 accumulation were not found in the majority of normal breast and colon tissue samples (Supplemental Figure 19A). Importantly, CASP3/DR is likely correlated with tumorigenesis in lung and colon tissues, because CASP3 expression was lower in malignancies compared with their adjacent normal tissues in microarray analyses of the paired normal/tumor (N/T) tissues (Supplemental Figure 19B). Furthermore, XIAP expression negatively correlated with CASP3 expression but was positively associated with p19/p12-CASP7 accumulation in clinical cancer samples (Supplemental Figure 20), which suggests that p19/p12-CASP7 forms complexes with XIAP. These findings elucidated the selectivity of I-Lys in killing CASP3/DR cells without inducing death in normal cells in vitro and in vivo.

We evaluated the clinical relevance of CASP3/DR by examining the association of p19/p12-CASP7 accumulation with prognosis in clinical cohorts of breast, lung, and colon cancer patients. We found that the signature of CASP3/DR, together with p19/p12-CASP7 accumulation, correlated significantly with reduced survival in patients with breast, lung, or colon cancer ($P \leq 0.001$; Figure 6C). In addition, multivariate statistical analyses revealed that breast, lung, and colon cancer patients with the signature of CASP3/DR combined with p19/p12-CASP7 accumulation harbored 5.3-, 3.9-, and 1.4-fold higher risk, respectively, for cancer recurrence and 10.4-, 3.4-, and 1.8-fold higher risk of death (Supplemental Table 3). These findings indicate that p19/p12-CASP7 accumulation could be a useful prognostic marker for cancer patients with CASP3/DR malignancies and that targeting the constitutively formed XIAP:p19/p12-CASP7 complex is a feasible strategy to selectively kill cancers with CASP3/DR.

microRNA let-7a-1 inhibits CASP3 expression, promoting multidrug resistance. To understand whether CASP3/DR causes chemoresistance in breast cancer patients, we analyzed the transcriptional profile of CASP3 expression in samples from patients with breast cancer prior to neoadjuvant chemotherapy (NAC) treatment (37). We found that CASP3/DR was highly associated with chemoresistance, especially in TNBCs (Figure 7A). Using stable clones generated from ER^+ T47D breast cancer cells overexpressing either the nontargeted control or microRNA let-7a-1 (*MIRLET7A1*), which posttranscriptionally represses *CASP3* expression (38), we found that *MIRLET7A1*-expressing T47D cells exhibited reduced CASP3 expression, but dramatic p19/p12-CASP7 accumulation, compared with control cells (Figure 7B). Furthermore, compared with the nontargeted control, *MIRLET7A1*-mediated CASP3/DR promoted multidrug resistance to tamoxifen, paclitaxel, and doxorubicin in T47D cells (Figure 7, C–E). Importantly, I-Lys killed the T47D cells with *MIRLET7A1*-induced CASP3/DR more efficiently than the control cells (Figure 7F). These data suggest a mechanism by which CASP3/DR and chemoresistance are mediated by *MIRLET7A1* and provide a rationale for targeting the PPI between p19/p12-CASP7 and XIAP to treat multidrug-resistant breast cancer cells.

Prevention of XIAP binding to p19/p12-CASP7 enhances chemotherapeutic killing of CASP3/DR cancer cells. Because XIAP binding to activated p19/p12-CASP7 inhibits STS-induced apoptosis in MCF-7 cells, we asked whether inhibiting the PPI between XIAP and p19/p12-CASP7 could enhance the cytotoxic effectiveness of STS or chemotherapeutics in CASP3/DR cancer cells. Interestingly, treatment of MCF-7 cells with I-Lys at a nontoxic concentration (0.2 μM) synergistically potentiated STS-induced apoptosis (Figure 7G). Combining STS or doxorubicin treatment with 0.2 μM I-Lys significantly enhanced their cytotoxic effectiveness in MCF-7 cells (Figure 7, H and I). This synergistic effect is likely due to the alkylation of pro-CASP7 by I-Lys, which prevented XIAP binding to the active form of p19/p12-CASP7 during STS- and chemotherapy-induced apoptosis in MCF-7 cells (Figure 8). Our results

demonstrated that preventing XIAP from binding to the emerging p19/p12-CASP7 upon apoptotic proteolysis of pro-CASP7 using a selective PPI inhibitor (e.g., I-Lys) could be an adjuvant for chemotherapy against malignancies with CASP3/DR.

Discussion

Here, we demonstrated that a synthetic small-molecule PPI blocker, I-Lys, which covalently binds to the Cys^{246} residue of p19/p12-CASP7, specifically disrupts the XIAP:p19/p12-CASP7 complexes that accumulate in CASP3/DR cancer cells. This disruption, in turn, induces release of p19/p12-CASP7, which directly triggers apoptosis in CASP3/DR cancer cells (Figure 8). Because CASP3/DR cancer cells rely on the activity of CASP7 to maintain cellular functions, e.g., proliferation (15), differentiation (16), and motility (17), XIAP:p19/p12-CASP7 complexes constitutively accumulate in resting CASP3/DR cancer cells, conferring cytotoxic selectivity for I-Lys. During the apoptotic demolition phase after treatment with I-Lys in CASP3/DR cells, the released p19/p12-CASP7 triggers proteolytic activation of downstream effectors, e.g., PARP, and activated pro-CASP7 processing in the late phase of apoptosis via the catalytic cleavage at Asp^{23} prior to internal cleavage by the apical enzymes, e.g., granzyme B (39). This process leads to increased production of p19/p12-CASP7, which is no longer restrained by XIAP because of the incorporation of I-Lys into pro-CASP7 at early time points; it also augments the tumoricidal effects of I-Lys on CASP3/DR cancer cells (Figure 8).

ER-α could induce *MIRLET7A1* transcription (our unpublished observations), which in turn repressed CASP3 expression (Figure 7B). Upon ER-α–induced CASP3/DR repression, breast cancer cells express CASP7, most likely through the binding of ER-α to its upstream promoter region (40), to compensate for the loss of cellular CASP3-dependent function. The accumulation of XIAP:p19/p12-CASP7 complex in nonapoptotic conditions then prevents apoptosis and provides the basis for the cytotoxic selectivity of I-Lys. Because CASP3 activation precedes CASP7 activation under both nonapoptotic and apoptotic conditions (18) in CASP3-expressing cells, e.g., in nontumor cells, restoring CASP3 expression in MCF-7 cells reduced the production of p19/p12-CASP7 in the resting stage (Supplemental Figure 10), thereby rendering the cells insensitive to I-Lys but sensitive to chemotherapy (41). Our study is the first to unveil a mechanism for CASP3/DR-associated chemoresistance in ER-α–expressing breast cancer cells; however, the precise mechanism underlying CASP3/DR and p19/p12-CASP7 accumulation in other cancer types, such as lung and colon cancers, requires further exploration.

Loss of CASP3, but not CASP7, in mice resulted in embryonic lethality (19, 21) and severe brain development defects (23), which demonstrates that CASP3 activity is necessary for maintaining cellular homeostasis in such processes as proliferation, differentiation, and motility in normal cells. Moreover, activated CASP3 has been shown to catalyze pro-CASP7 activation and processing into p19/p12-CASP7 by removing the N-terminal pseudopeptide via cleavage of the Asp^{23} residue prior to internal cleavage by apical caspases during apoptosis (42). XIAP binds avidly to activated CASP3 not only to prevent apoptosis, but also to inhibit CASP7 activation in response to nonapoptotic stimuli. Therefore, the intracellular accumulation of the XIAP:p19/p12-CASP7 complex might be very rare in nontumorigenic cells. Indeed, targeting the PPI in the XIAP:p19/p12-CASP7 complex with I-Lys robustly killed *CASP3*-null MCF-7 breast cancer cells without affecting the growth of normal *CASP3*-expressing MCF-10A mammary epithelium cells. Similarly, I-Lys treatment selectively inhibited in vivo tumor growth of MCF-7 cells without inducing other physiological changes in the tumor-bearing mice.

Because XIAP overexpression correlates strongly with cancer progression and chemoresistance, small-molecule XIAP antagonists (43–45) and SMAC mimetics (46–48) have been developed to inhibit the interaction of XIAP with CASP9 and CASP3 and kill malignant tumor cells. However, these agents are toxic to normal cells due to off-target effects, such as inhibition of the growth of hematopoietic progenitor/stem cells (49); these effects are likely caused by the interaction of XIAP with active CASP3, which is required for preventing apoptosis in normal proliferating cells (15). In contrast, I-Lys selectively hindered the PPI of the full-length XIAP and its linker-BIR2 domain with p19/p12-CASP7, but not with active CASP3, as shown by in vitro binding assays, and exhibited cytotoxic selectivity for CASP3/DR cancer cells in vitro and in vivo, owing to the massive accumulation of the XIAP:p19/p12-CASP7 complex.

NAC, which combines several anticancer agents, such as paclitaxel with fluorouracil, doxorubicin, and cyclophosphamide, has been used as the standard treatment for patients with TNBCs (50) and ER^+ breast cancer (51) to achieve a complete pathological response. However, approximately 70% of breast cancer patients are insensitive to NAC treatment (50). Here, we provided evidence for CASP3/DR in TNBCs (Figure 7A) and demonstrated that CASP3/DR conferred drug resistance to tamoxifen, paclitaxel, and doxorubicin (Supplemental Figure 1 and Supplemental Table 1), which was likely responsible for the poor prognosis of cancer patients. Therefore, disrupting the XIAP:p19/p12-CASP7 complex represents an attractive strategy to combat multidrug-resistant cancers (Figure 7F). Another practical application of this study may be adjuvant use of I-Lys at low concentrations to enhance the effect of doxorubicin and other apoptosis-inducing chemotherapeutics in cancer therapy, which would hinder the binding of XIAP to p19/p12-CASP7 in apoptotic CASP3/DR cancer cells (Figure 7I).

In summary, our results demonstrated that CASP3/DR occurs in multiple cancer types, presumably due to posttranscriptional repression by *MIRLET7A1*, which correlates with poor prognosis for patients. Fortunately, targeting the XIAP:p19/p12-CASP7 complex using PPI inhibitors (e.g., I-Lys) appeared to selectively kill CASP3/DR cancer cells without adverse side effects in normal cells, which suggests that XIAP:p19/p12-CASP7 is a viable target for chemotherapies designed to treat malignancies with CASP3/DR.

Methods

Reagents. All chemicals used for synthesis were purchased from Sigma-Aldrich. The Fluorometric Caspase Assay kit was from BioVision. Antibodies against CASP3, pro-CASP7, p19-CASP7, CASP9, XIAP, and PARP were from Cell Signaling. Antibodies against XIAP (for immunoprecipitation), GAPDH, and GFP were from Santa Cruz Biotechnology. The CASP7 inhibitor MPS and the PARP inhibitor IAB were from Calbiochem (Merck Biosciences). pET-28a and pIRES2-EGFP vectors were from Novagen (Merck Biosciences) and Clontech, respectively.

Cell culture. MCF-7 cells were obtained from the Bioresource Collection and Research Centre (BCRC, Hsinchu, Taiwan) and cultivated in MEM supplemented with 10% FBS. Normal MCF-10A mammary cells and BT-483, T47D, and Hs578T breast cancer cells were obtained from M. Hsiao (Genomics Research Center, Academia Sinica, Taipei, Taiwan). AU-565, SKBR-3, MDA-MB-231, and MDA-MB-157 cells were gifts of

W.-H. Lee (Genomics Research Center, Academia Sinica, Taipei, Taiwan). MCF-10A cells were maintained in DMEM/F12 medium with 5% horse serum and supplemented with 20 ng/ml epithelium growth factor, 0.5 mg/ml hydrocortisone, 100 ng/ml cholera toxin, and 10 μg/ml insulin. BT483, T47D, AU-565, and SKBR3 cells were cultured in RPMI-1640 medium with 10% FBS. Hs578T cells were cultured in DMEM/F12 medium with 10% FBS. MDA-MB231 and MDA-MB157 cells were maintained in DMEM with 10% FBS. All cells were maintained in 5% CO_2 at 37°C.

Confocal microscopy. Cells (1×10^5) were grown on poly-L-lysine–treated round cover slides (22 mm diameter, 0.17 mm thick; Sigma-Aldrich). After treatment with I-Lys-B at 1 μM for 2 hours, cells were fixed with 4% formaldehyde for 15 minutes at room temperature. After 2 washes with PBS, cells were treated with 95% EtOH and 5% CH_3COOH at –20°C for 15 minutes. Then, cells were washed twice with PBS and blocked with 2% BSA and 0.1% Triton X-100 for 2 hours at room temperature. Subsequently, cells were incubated with the CASP7 antibody overnight at 4°C. After 3 washes with PBS, cells were incubated with a biotin-conjugated secondary antibody (DAKO) for 1 hour at room temperature. After several washes, cells were incubated with fluorescein-conjugated avidin complex (Vector Laboratories) for 30 minutes at room temperature. For nuclear staining, cells were incubated with PI (10 μg/ml) for 15 minutes at room temperature. After mounting on slides with 50% glycerol and TBS (pH 7.0), cells were observed using the LSM510 Confocal Microscope System (Carl Zeiss MicroImaging Inc.).

PI-based flow cytometric analysis. Cells (6×10^5) were fixed in 70% ice-cold EtOH for 30 minutes at room temperature. The cells were then washed once with PBS and incubated with the PI staining solution (0.1% BSA, 0.1% RNase A, and 20 ng/ml PI in PBS) for 30 minutes at room temperature in the dark. After incubation, cells were analyzed by flow cytometry to assess DNA content. The cells that accumulated in the sub-G_0 region were defined as apoptotic cells; DNA fragmentation verified that the cytotoxic effect of I-Lys on MCF-7 cells was via apoptotic cell death.

MTT assay. Cells (2×10^5/ml) were seeded into a 96-well culture plate. After an incubation period, 10 μl of 3-(4,5-dimethylthiazol-2-yl)-2,5-diphenyltetrazolium bromide (MTT; Molecular Probes) stock solution was added to each well. Conversion of MTT to formazan by viable cells was conducted at 37°C for another 4 hours. After the reaction, 100 μl DMSO solution was added to each well to solubilize the formazan precipitates. To calculate cell survival rates, the amount of formazan was determined by optical density measurement at 540 nm using an ELISA reader.

Determination of in vitro and real-time intracellular DEVDase activity. The caspase activity assay was performed using a commercial kit according to the manufacturer's protocol (BioVision). To determine real-time CASP7 activity, cells were cultured in 6-well culture plates containing 9-mm × 22-mm cover slips coated with poly-L-lysine (Sigma-Aldrich). After 2 days of culture, cells were pretreated with 1 μM fluorogenic DEVD substrate PhiPhiLux-G_1D_2 (OncoImmunin) for 1 hour at 37°C. Subsequently, cover slips were transferred to a 4-ml quartz cuvette containing 2 ml Reaction Buffer (OncoImmunin). Analysis of real-time CASP7 activity was performed in a Hitachi F-4500 Fluorescence Spectrophotometer using excitation and emission wavelengths at 505 and 530 nm, respectively. A designated amount of I-Lys or staurosporine was added using a microinjection syringe when the baseline was stable. The level of DEVDase activity is presented as the ratio of fluorescence intensity, subtracting that of time 0.

Western blot analysis. Protein extracts (100 μg) were boiled for 5 minutes in SDS sample buffer (62.5 mM Tris pH 6.7, 1.25% SDS, 12.5% glycerol, and 2.5% β-mercaptoethanol) and separated on 12% SDS-PAGE gels. After being transferred to a PVDF membrane, the membrane was incubated with antibodies against pro-CASP3, pro-CASP7, p19-CASP7, XIAP, GFP, and GAPDH. Immunoreactive bands were visualized using an ECL system (Amersham Bioscience).

Immunoprecipitation. Cell lysates (500 μg) were diluted in 1 ml cell lysis buffer (10 mM Tris-HCl pH 7.4, 140 mM NaCl, 3 mM $MgCl_2$, 2 mM EDTA, 5 mM EGTA, 0.5% Triton X-100, and 4% protease inhibitor cocktail [Merck Biosciences]) and incubated with rabbit anti–p19-CASP7 or mouse anti-XIAP antibody (2 μg of each) overnight at 4°C, followed by precipitation with 20 μl protein A–agarose beads for 1 hour at 4°C. Immunoprecipitates were analyzed by SDS-PAGE/Western blotting using XIAP and p19-CASP7 antibodies. To avoid the appearance of the Ig heavy and light chain bands in the immunoprecipitates, we used horseradish peroxidase–conjugated anti-mouse IgG light chain (Jackson ImmunoResearch Laboratories) and conformation-specific anti-rabbit IgG (Cell Signaling) antibodies to detect the XIAP and p19-CASP7 antibodies, respectively, in Western blotting. In addition, blots were stripped using a commercial kit (Millipore) and reprobed with anti-XIAP or anti–p19-CASP7 antibodies.

Lentiviral shRNA infection. Cells at 50% confluence that were grown in 6-well plates were fed with fresh media containing 5 μg/ml polybrene (Santa Cruz) before being infected with lentivirus containing *CASP7* shRNA; infection was conducted overnight to promote the establishment of stable *CASP7*-knockdown cells. To select cells stably expressing *CASP7* shRNA, cells were cultured in the presence of puromycin (10 μg/ml; Santa Cruz) for 24 hours. The puromycin-resistant cells were split into 96-well plates at a density of 1 cell/well to generate a cell line stably expressing *CASP7* shRNA.

RT-PCR. Total RNA was extracted from cells using a RNA extraction kit (Genomics). Aliquots (5 μg) of total RNA were treated with M-MLV reverse transcriptase (Invitrogen) and amplified with Taq-polymerase (MDBIO) using the following paired primers: *CASP3* forward, 5′-ATGGAGAACACTGAAAACTCAGTGG-3′; *CASP3* reverse, 5′-GTGATAAAAATAGAGTTCTTTTGTGAGCAT-3′; *CASP7* forward, 5′-ATGGCAGATGATCAGGGCTGT-3′; *CASP7* reverse, 5′-CTATTGACTGAAGTAGAGTTCCTTGGTG-3′; *GAPDH* forward, 5′-AGGTCGGAGTCAACGGATTTG-3′; *GAPDH* reverse, 5′-GTGATGGCATGGACTGTGGT-3′.

Identification of I-Lys– and VAD-labeled proteins in MCF-7 cells. Cell lysates (10 mg) were diluted in 1 ml binding buffer (25 mM Tris-HCl, pH 7.4, and 150 mM NaCl) and were precleared by incubating with 0.1 ml streptavidin-sepharose beads (Sigma-Aldrich) for 1 hour at 4°C with gentle rotation prior to incubation with 200 μM I-Lys-B at 4°C overnight with gentle rotation. The I-Lys-B–treated cell lysates were purified by affinity chromatography using a HiTrap Streptavidin affinity column according to the manufacturer's guidelines (GE Healthcare). In other experiments, 2×10^5 cells/ml were pretreated with the pan-caspase inhibitor biotin-VAD-fmk (BioVision) (52) at a concentration of 2.5 μM for 1 hour prior to treatment with I-Lys or STS (1 μM each) at the designated time points. Aliquots of cell lysates (1 mg) were incubated with 0.1 ml streptavidin-sepharose beads (Sigma-Aldrich) for 1 hour at 4°C with gentle rotation. Pellets were analyzed by Western blotting using anti–p19-CASP7 antibody.

Plasmid construction, site-directed mutagenesis, and stable clone generation. For the *E. coli* system, the human cDNA sequences encoding CASP3 (NM_004346.3), CASP7 (NM_033339.3), and XIAP (NM_0011167.2) from commercial cDNA clones (Origene) were used as templates to construct full-length CASP3 and CASP7 and the linker-BIR2 domain (residues 124–240) of XIAP using the sticky-end PCR method with EcoRI/XhoI restriction sites. CASP3 and CASP7 were introduced into the modified pET-28a vector (53), whereas the XIAP linker-BIR2 domain was cloned into the pGEX-4T1 vector. Paired primers were as follows: CASP3 1 forward, 5′-AATTCATGGAGAACACTGAAAACTCAGTGG-3′; CASP3 1 reverse, 5′-GGTGATAAAAATAGAGTTCTTTTGTGAGCAT-3′; CASP3 2 forward, 5′-CATGGAGAACACTGAAAACTCAGTGG-3′; CASP3 2 reverse, 5′-TCGAGGTGATAAAAATAGAGTTCTTTTGTGAGCAT-3′; CASP7 1 forward, 5′-AATTCATGGCAGATGATCAGGGCTGT-3′; CASP7 1 reverse,

5′-GCTATTGACTGAAGTAGAGTTCCTTGGTG-3′; CASP7 2 forward, 5′-CATGGCAGATGATCAGGGCTGT-3′; CASP7 2 reverse, 5′-TCGAGCTATTGACTGAAGTAGAGTTCCTTGGTG-3′; linker-BIR2 1 forward, 5′-AATTCAGAGATCATTTTGCCTTAGACAGGC-3′; linker-BIR2 1 reverse, 5′-GATCAGATTCACTTCGAATATTAAGATTCC-3′; linker-BIR2 2 forward, 5′-CAGAGATCATTTTGCCTTAGACAGGC-3′; linker-BIR2 2 reverse, 5′-TCGAGGATCAGATTCACTTCGAATATTAAGATTCC-3′.

For the mammalian system, the sticky-end PCR products of full-length CASP3 and CASP7 with XhoI/EcoRI restriction sites were inserted into the pIRES2-EGFP vector. Paired primers were as follows: CASP3 1 forward, 5′-TCGAGATGGAGAACACTGAAAACTCAGTG-3′; CASP3 1 reverse, 5′-CTTAGTGATAAAAATAGAGTTCTTTTGTGAG-3′; CASP3 2 forward, 5′-GATGGAGAACACTGAAAACTCAGTG-3′; CASP3 2 reverse, 5′-AATTCTTAGTGATAAAAATAGAGTTCTTTTGTGAG-3′; CASP7 1 forward, 5′-TCGAGATGGCAGATGATCAGGGCTGT-3′; CASP7 1 reverse, 5′-CCTATTGACTGAAGTAGAGTTCCTTGGTG-3′; CASP7 2 forward, 5′-GATGGCAGATGATCAGGGCTGT-3′; CASP7 2 reverse, 5′-AATTCCTATTGACTGAAGTAGAGTTCCTTGGTG-3′. To generate the CASP7/D23A and CASP7/C246S mutants, the pIRES2-EGFP/CASP7 plasmid was used as a DNA template and subjected to site-directed mutagenesis using the QuikChange II Kit (Stratagene) using the following paired primers: CASP7/D23A forward, 5′-AAATGAAGATTCAGTGGCTGCTAAGCCAGACCGGT-3′; CASP7/D23A reverse, 5′-ACCGGTCTGGCTTAGCAGCCACTGAATCTTCATTT-3′; CASP7/C246S forward, 5′-GTGCAAGCCCTCTCCTCCATCCTGGAG-3′; CASP7/C246S reverse, 5′-CTCCAGGATGGAGGAGAGGGCTTGCAC-3′. The identities of the individual clones were verified through double-strand plasmid sequencing.

To generate MCF-7 cells stably expressing WT *CASP3*, WT *CASP7*, or *CASP7* mutant constructs, MCF-7 cells were transfected with 1 μg of each plasmid using the Lipofectamine delivery system (Invitrogen) for 24 hours. To generate T47D cells that stably expressed *MIRLET7A1*, T47D cells were transfected with the pCMV-MIR vector (Origene) containing a nontargeted control or *MIRLET7A1* (1 μg each) for 24 hours. After selection with the G418 antibiotic, cells were seeded into 96-well plates at a density of 5 cells/ml to yield single colonies. Cells stably expressing *CASP3*, *CASP7*, or *CASP7* mutants were monitored by EGFP expression.

Protein expression and purification. Recombinant proteins including C-terminally 6-His–tagged p19/p12-CASP7 and N-terminally GST-tagged full-length XIAP and the linker-BIR2 (residues 124–240) domain of XIAP were overexpressed in *E. coli* strain BL-21(DE3). To produce pro-CASP7 and active p19/p12-CASP7, bacterial hosts were treated with IPTG (0.2 mM) for 2 and 18 hours, respectively (54). N-terminal cleavage at the Asp^{23} residue was identified by N-terminal amino acid sequencing using Edman degradation. The soluble fraction containing the recombinant proteins from the *E. coli* lysate was purified over a Ni-NTA or glutathione-coated column according to the manufacturer's protocol (Amersham Biosciences).

Identification of I-Lys–alkylated Cys residues in CASP7. Recombinant CASP7 protein (200 μg) was diluted in 0.5 ml binding buffer as described above and incubated with 10 μM I-Lys-Dan overnight at 4°C with gentle rotation in the dark. The labeled recombinant CASP7 protein (30 μg) was subjected to electrophoresis on a 12% SDS-PAGE gel. The fluorescent protein band, visualized under a UV lamp, was excised from the gel and subjected to in-gel chymotryptic digestion and liquid chromatography–electrospray ionization–tandem mass spectrometric (LC-ESI-MS) analysis. For protein fingerprinting analysis, the resultant *m/z* values of each peptide fragment were compared with the predicted molecular weight of the peptide fragments derived from CASP7 with an alkylated Cys.

Assessment of in vitro BIR2 interaction with active CASP3 or p19/p12-CASP7. Recombinant active CASP3 or p19/p12-CASP7 (0.2 μg) was preincubated with GST or GST-tagged XIAP linker-BIR2 domain (0.2 μg) for 1 hour at 4°C to allow for complex formation. I-Lys (50 or 100 μM) was then added to the mixture. After 1 hour of incubation, active CASP3 or p19/p12-CASP7 bound to GST or GST-tagged linker-BIR2 was precipitated using glutathione-Sepharose beads (Amersham Biosciences). After several washes with HEPES buffer (10 mM HEPES, 142 mM KCl, 1 mM EGTA, 1 mM dithiothreitol, 0.2% Nonidet P-40 pH 7.5), pellets were analyzed by immunoblotting with p19-CASP7 or GST antibody.

Microarray analysis. Transcriptional profiling results for *CASP3* were obtained from GEO (accession nos. GSE20271 and GSE10890). Relative mRNA expression levels were normalized to the median and presented as $\log_2$ values.

Computer modeling. Molecular docking of I-Lys with pro-CASP7 (PDB 1K86) or p19/p12-CASP7 (PDB 1I51) was evaluated using GEMDOCK software (55). Intermolecular interactions between docked compound and protein residues were analyzed using Swiss-PdbViewer 3.7 software.

Animal model. Immunodeficient NOD-SCID mice (6–7 weeks of age) were obtained from the Jackson Laboratory and housed in the animal room of the Genomics Research Center of Academia Sinica under a constant 12-hour light/12-hour dark cycle and fed with Laboratory Irradiated Rodent Diet 5058 (LabDiet). MCF-7, MDA-MB157, and MDA-MB231 cells (5×10^5) were suspended in 50 μl PBS and injected subcutaneously into the abdominal fat pad of each mouse as an orthotopic implantation. 1 day before MCF-7 cell implantation, mice were fed a 17β-estradiol pellet (Innovative Research of America). After implantation, mice were randomly assigned to 3 groups ($n = 8$) that received vehicle control or 5 or 25 mg/kg I-Lys in 100 μl PBS containing 0.1% DMSO 2 times per week (every 3–4 days) by intraperitoneal injection. Animal body weights were measured before drug treatment. Subcutaneous tumors were measured every week using calipers, and their volumes were calculated using the standard formula $(w \times l^2)/2$. Mice were sacrificed 5 weeks after injection with I-Lys to harvest the serum and tissues for further serological and histological examination, respectively. A portion of each tumor was frozen in liquid nitrogen and stored at –80°C until needed for analysis of the compounds in the tumors, and the remainder was fixed in 10% formalin overnight. Serum samples were analyzed by the Taiwan Mouse Clinic of Taiwan Phenotyping Center.

IHC. Paraffin-embedded tumor sections (3 μm thick) were heated and deparaffinized using xylene, rehydrated in a graded series of ethanol steps, and washed in tap water. Antigen retrieval was performed using the Target Retrieval Solution (DAKO) in a Decloaking Chamber (Biocare Medical). Endogenous peroxidase activity was quenched using hydrogen peroxide. Sections were incubated with anti–Ki-67 (DAKO), anti-CASP3 (1:500; Millipore), anti–p19/p12-CASP7 (1:1,000; Imgenex), or anti-XIAP (1:500; Genetex) antibodies at 4°C overnight in a humid chamber. The Vectastain ABC peroxidase system (Vector Laboratories) was used to detect the reaction products. In situ detection of apoptotic cells was carried out using the TUNEL assay kit according to the manufacturer's protocol (Merck Biosciences). IHC images were captured with an Olympus DP70 camera attached to an Olympus BX51 microscope using a ×40 objective.

Clinical samples. Breast, lung, and colon cancer tissues were from Taipei Medical University–managed Wan Fang Hospital, Kaohsiung Medical University Hospital, and Taipei Medical University Hospital, respectively. Patient information, including gender, age, and histopathological diagnoses, was collected. The surgical specimens had been fixed in formalin and embedded in paraffin before they were archived. We used the archived specimens for IHC staining. Patient follow-up was carried out for up to 60 months for the breast and lung cancer patients and 200 months for the colon cancer patients. A 4-point staining intensity scoring system was devised to determine the relative expression of

CASP3, p19/p12-CASP7, and XIAP in cancer specimens; the staining intensity score ranged from 0 (no expression) to 3 (maximum expression). All IHC staining results were reviewed and scored independently by 2 pathologists.

Statistics. Pearson rank correlations were determined for comparisons between CASP3 and p19/p12-CASP7 IHC staining. Pearson χ^2 tests were used to analyze the association of low- and high-level p19/p12-CASP7 staining with different TNM stages in a cohort of subjects with colon cancer. Kaplan-Meier analysis was used to evaluate the association of CASP3 expression with cancer patient survival data, and log-rank tests were performed to determine its statistical significance. Cox proportional hazards regression was used to test the prognostic significance of the factors indicated in Supplemental Table 3 in multivariate models. Statistical analysis of 3 independent experiments was performed using nonparametric Mann-Whitney test. All statistical tests were 2-sided, and a *P* value less than 0.05 was considered significant.

Study approval. The study was initiated after obtaining Institutional Review Board approval from Taipei Medical University Hospital (Taipei, Taiwan) and Kaohsiung Medical University Hospital (Kaohsiung, Taiwan), and experiments were performed in compliance with these protocols. All subjects provided informed consent prior to participation, and specimens were deidentified prior to analysis. All animal work was conducted according to protocols approved by the Institutional Animal Care and Use Committee of Academia Sinica.

Acknowledgments

The authors thank Wen-Hwa Lee and Jin-Yuh Shew for providing the breast cancer cell lines AU-565, SKBR-3, MDA-MB231, and MDA-MB157; Zack Tzan Fang for help with animal experiments; Tracy Tsai for help with IHC experiments; the Taiwan Mouse Clinic (funded by the National Research Program for Biopharmaceuticals [NRPB] at the National Science Council [NSC] of Taiwan) for technical support in serological experiments. This study was supported by Academia Sinica and the National Science Council of Taiwan, ROC.

Received for publication November 21, 2012, and accepted in revised form June 21, 2013.

Address correspondence to: Po-Huang Liang, Institute of Biological Chemistry, Academia Sinica, 128 Academia Road, Taipei, 11529, Taiwan. Phone: 886.2.3366.4069; Fax: 886.2.2363.5038; E-mail: phliang@gate.sinica.edu.tw.

1. Devarajan E, et al. Down-regulation of caspase 3 in breast cancer: a possible mechanism for chemoresistance. *Oncogene*. 2002;21(57):8843–8851.
2. Sun Y, et al. Differential caspase-3 expression in noncancerous, premalignant and cancer tissues of stomach and its clinical implication. *Cancer Detect Prev*. 2006;30(2):168–173.
3. Winter RN, Kramer A, Borkowski A, Kyprianou N. Loss of caspase-1 and caspase-3 protein expression in human prostate cancer. *Cancer Res*. 2001;61(3):1227–1232.
4. Volm M, Koomagi R. Prognostic relevance of c-Myc and caspase-3 for patients with non-small cell lung cancer. *Oncol Rep*. 2000;7(1):95–98.
5. Oudejans JJ, et al. Absence of caspase 3 activation in neoplastic cells of nasopharyngeal carcinoma biopsies predicts rapid fatal outcome. *Mod Pathol*. 2005;18(7):877–885.
6. Andressakis D, Lazaris AC, Tsiambas E, Kavantzas N, Rapidis A, Patsouris E. Evaluation of caspase-3 and caspase-8 deregulation in tongue squamous cell carcinoma, based on immunohistochemistry and computerised image analysis. *J Laryngol Otol*. 2008;122(11):1213–1218.
7. Zygouris P, et al. Evaluation of combined h-TERT, bcl-2, and caspases 3 and 8 expression in cutaneous malignant melanoma based on tissue microarrays and computerized image analysis. *J BUON*. 2007;12(4):513–519.
8. Huang H, et al. Expression and prognostic significance of osteopontin and caspase-3 in hepatocellular carcinoma patients after curative resection. *Cancer Sci*. 2010;101(5):1314–1319.
9. Iolascon A, et al. Caspase 3 and 8 deficiency in human neuroblastoma. *Cancer Genet Cytogenet*. 2003;146(1):41–47.
10. de Heer P, et al. Caspase-3 activity predicts local recurrence in rectal cancer. *Clin Cancer Res*. 2007;13(19):5810–5815.
11. de Oca J, et al. Caspase-3 activity, response to chemotherapy and clinical outcome in patients with colon cancer. *Int J Colorectal Dis*. 2008;23(1):21–27.
12. Gronda M, et al. Assessment of the downstream portion of the mitochondrial pathway of caspase activation in patients with acute myeloid leukemia. *Apoptosis*. 2005;10(6):1285–1294.
13. Blanc C, et al. Caspase-3 is essential for procaspase-9 processing and cisplatin-induced apoptosis of MCF-7 breast cancer cells. *Cancer Res*. 2000;60(16):4386–4390.
14. Hui KK, Kanungo AK, Elia AJ, Henderson JT. Caspase-3 deficiency reveals a physiologic role for Smac/DIABLO in regulating programmed cell death. *Cell Death Differ*. 2011;18(11):1780–1790.
15. Paulsen M, et al. Interaction with XIAP prevents full caspase-3/-7 activation in proliferating human T lymphocytes. *Eur J Immunol*. 2008;38(7):1979–1987.
16. Szymczyk KH, Freeman TA, Adams CS, Srinivas V, Steinbeck MJ. Active caspase-3 is required for osteoclast differentiation. *J Cell Physiol*. 2006;209(3):836–844.
17. Acarin L, Villapol S, Faiz M, Rohn TT, Castellano B, González B. Caspase-3 activation in astrocytes following postnatal excitotoxic damage correlates with cytoskeletal remodeling but not with cell death or proliferation. *Glia*. 2007;55(9):954–965.
18. Walsh JG, Cullen SP, Sheridan C, Lüthi AU, Gerner C, Martin SJ. Executioner caspase-3 and caspase-7 are functionally distinct proteases. *Proc Natl Acad Sci U S A*. 2008;105(35):12815–12819.
19. Kuida K, et al. Decreased apoptosis in the brain and premature lethality in CPP32-deficient mice. *Nature*. 1996;384(6607):368–372.
20. Gafni J, Cong X, Chen SF, Gibson BW, Ellerby LM. Calpain-1 cleaves and activates caspase-7. *J Biol Chem*. 2009;284(37):25441–25449.
21. Lakhani SA, et al. Caspases 3 and 7: key mediators of mitochondrial events of apoptosis. *Science*. 2006;311(5762):847–851.
22. Lee AT, Azimahtol HL, Tan AN. Styrylpyrone Derivative (SPD) induces apoptosis in a caspase-7-dependent manner in the human breast cancer cell line MCF-7. *Cancer Cell Int*. 2003;3(1):16.
23. Houde C, et al. Caspase-7 expanded function and intrinsic expression level underlies strain-specific brain phenotype of caspase-3-null mice. *J Neurosci*. 2004;24(44):9977–9984.
24. Zheng TS, et al. Deficiency in caspase-9 or caspase-3 induces compensatory caspase activation. *Nat Med*. 2000;6(11):1241–1247.
25. Twiddy D, Cohen GM, Macfarlane M, Cain K. Caspase-7 is directly activated by the approximately 700-kDa apoptosome complex and is released as a stable XIAP-caspase-7 approximately 200-kDa complex. *J Biol Chem*. 2006;281(7):3876–3888.
26. Suzuki Y, Nakabayashi Y, Nakata K, Reed JC, Takahashi R. X-linked inhibitor of apoptosis protein (XIAP) inhibits caspase-3 and -7 in distinct modes. *J Biol Chem*. 2001;276(29):27058–27063.
27. Yang PM, Tseng HH, Peng CW, Chen WS, Chiu SJ. Dietary flavonoid fisetin targets caspase-3-deficient human breast cancer MCF-7 cells by induction of caspase-7-associated apoptosis and inhibition of autophagy. *Int J Oncol*. 2012;40(2):469–478.
28. Yamasaki-Miyamoto Y, Yamasaki M, Tachibana H, Yamada K. Fucoidan induces apoptosis through activation of caspase-8 on human breast cancer MCF-7 cells. *J Agric Food Chem*. 2009;57(18):8677–8682.
29. Chou CC, Wu YC, Wang YF, Chou MJ, Kuo SJ, Chen DR. Capsaicin-induced apoptosis in human breast cancer MCF-7 cells through caspase-independent pathway. *Oncol Rep*. 2009;21(3):665–671.
30. Lin YF, Tsai WP, Liu HG, Liang PH. Intracellular β-tubulin/chaperonin containing TCP1-β complex serves as a novel chemotherapeutic target against drug-resistant tumors. *Cancer Res*. 2009;69(17):6879–6888.
31. Lin YF, Lee YF, Liang PH. Targeting β-tubulin: CCT-β complexes incurs Hsp90- and VCP-related protein degradation and induces ER stress-associated apoptosis by triggering capacitative Ca(2+) entry, mitochondrial perturbation and caspase overactivation. *Cell Death Dis*. 2012;3:e434.
32. Germain M, Affar EB, D'Amours D, Dixit VM, Salvesen GS, Poirier GG. Cleavage of automodified poly(ADP-ribose) polymerase during apoptosis. Evidence for involvement of caspase-7. *J Biol Chem*. 1999;274(40):28379–28384.
33. Xue LY, Chiu SM, Oleinick NL. Staurosporine-induced death of MCF-7 human breast cancer cells: a distinction between caspase-3-dependent steps of apoptosis and the critical lethal lesions. *Exp Cell Res*. 2003;283(2):135–145.
34. Lee D, et al. Potent and selective nonpeptide inhibitors of caspases 3 and 7. *J Med Chem*. 2001; 44(12):2015–2026.
35. Scott FL, Denault JB, Riedl SJ, Shin H, Renatus M, Salvesen GS. XIAP inhibits caspase-3 and -7 using two binding sites: evolutionarily conserved mechanism of IAPs. *EMBO J*. 2005;24(3):645–655.
36. Lee SJ, et al. Metronomic activity of CD44-targeted hyaluronic acid-paclitaxel in ovarian carcinoma. *Clin Cancer Res*. 2012;18(15):4114–4121.
37. Tabchy A, et al. Evaluation of a 30-gene paclitaxel, fluorouracil, doxorubicin, and cyclophosphamide chemotherapy response predictor in a multicenter randomized trial in breast cancer. *Clin Cancer Res*. 2010;16(21):5351–5361.
38. Tsang WP, Kwok TT. Let-7a microRNA suppresses therapeutics-induced cancer cell death by targeting

caspase-3. *Apoptosis*. 2008;13(10):1215–1222.
39. Yang X, et al. Granzyme B mimics apical caspases. Description of a unified pathway for trans-activation of executioner caspase-3 and -7. *J Biol Chem*. 1998;273(51):34278–34283.
40. Ross-Innes CS, et al. Differential oestrogen receptor binding is associated with clinical outcome in breast cancer. *Nature*. 2012;481(7381):389–393.
41. Friedrich K, et al. Overexpression of caspase-3 restores sensitivity for drug-induced apoptosis in breast cancer cell lines with acquired drug resistance. *Oncogene*. 2001;20(22):2749–2760.
42. Denault JB, Salvesen GS. Human caspase-7 activity and regulation by its N-terminal peptide. *J Biol Chem*. 2003;278(36):34042–34050.
43. Wu TY, Wagner KW, Bursulaya B, Schultz PG, Deveraux QL. Development and characterization of non-peptidic small molecule inhibitors of the XIAP/caspase-3 interaction. *Chem Biol*. 2003;10(8):759–767.
44. Oost TK, et al. Discovery of potent antagonists of the antiapoptotic protein XIAP for the treatment of cancer. *J Med Chem*. 2004;47(18):4417–4426.
45. Schimmer AD, Dalili S, Batey RA, Riedl SJ. Targeting XIAP for the treatment of malignancy. *Cell Death Differ*. 2006;13(2):179–188.
46. Gao Z, et al. A dimeric Smac/diablo peptide directly relieves caspase-3 inhibition by XIAP. Dynamic and cooperative regulation of XIAP by Smac/Diablo. *J Biol Chem*. 2007;282(42):30718–30727.
47. Lu J, et al. SM-164: a novel, bivalent Smac mimetic that induces apoptosis and tumor regression by concurrent removal of the blockade of cIAP-1/2 and XIAP. *Cancer Res*. 2008;68(22):9384–9393.
48. Dineen SP, et al. Smac mimetic increases chemotherapy response and improves survival in mice with pancreatic cancer. *Cancer Res*. 2010; 70(7):2852–2861.
49. Schimmer AD, et al. Small-molecule antagonists of apoptosis suppressor XIAP exhibit broad antitumor activity. *Cancer Cell*. 2004;5(1):25–35.
50. Balko JM, et al. Profiling of residual breast cancers after neoadjuvant chemotherapy identifies DUSP4 deficiency as a mechanism of drug resistance. *Nat Med*. 2012;18(7):1052–1059.
51. Ikeda H, et al. Combination treatment with fulvestrant and various cytotoxic agents (doxorubicin, paclitaxel, docetaxel, vinorelbine, and 5-fluorouracil) has a synergistic effect in estrogen receptor-positive breast cancer. *Cancer Sci*. 2011;102(11):2038–2042.
52. Jost PJ, et al. XIAP discriminates between type I and type II FAS-induced apoptosis. *Nature*. 2009;460(7258):1035–1039.
53. Wang HM, et al. Parallel gene cloning and protein production in multiple expression systems. *Biotechnol Prog*. 2009;25(6):1582–1586.
54. Stennicke HR, Salvesen GS. Caspases: preparation and characterization. *Methods*. 1999;17(4):313–319.
55. Yang JM, Chen CC. GEMDOCK: a generic evolutionary method for molecular docking. *Proteins*. 2004;55(2):288–304.